JOURNAL OF GEOPHYSICAL RESEARCH, VOL. 95, NO. D11, PAGES 18,687–18,703, OCTOBER 20, 1990

Seasonal Variation of Cloud Radiative Forcing Derived From the Earth Radiation Budget Experiment

E. F. HARRISON,[1] P. MINNIS,[1] B. R. BARKSTROM,[1] V. RAMANATHAN,[2] R. D. CESS,[3] AND G. G. GIBSON[4]

The NASA Earth Radiation Budget Experiment (ERBE), flying aboard multiple satellites, is providing new insights into the climate system. Monthly averaged clear-sky and cloudy sky flux data derived from the ERBE are used to assess the impact of clouds on the Earth's radiation balance. This impact is examined in terms of three quantities: longwave, shortwave, and net cloud forcing. Overall, clouds appear to cool the Earth-atmosphere system. The global mean cooling varied from 14 to 21 W m^{-2} between April 1985 and January 1986. Hemispherically, the longwave and shortwave cloud forcing nearly cancel each other in the winter hemisphere, while in the summer the negative shortwave cloud forcing is significantly lower than the longwave cloud forcing, producing a strong cooling. Thus clouds significantly reduce the seasonal changes in the net radiative heating of the planet. This reduction is particularly strong over the mid- and high-latitude oceans, where they reduce the summer and spring solar heating by as much as 100–150 W m^{-2}. In the low latitudes, the longwave and shortwave cloud forcing reach peak values over the convectively disturbed regions and tend to offset each other to a large extent. This feature, when combined with the large cooling effect over mid- and high-latitude oceans, leads to the conclusion that clouds significantly reduce the equator-to-pole radiative heating gradient of the planet during spring and summer. In the tropical convective regions the large magnitudes of the shortwave and longwave forcing and the near cancellation of the two suggest that clouds have a significant influence on the vertical distribution of heating between the atmosphere and the surface. Thus the ERBE data reveal that globally, hemispherically, and zonally, clouds have a significant effect on the radiative heating gradients. Comparisons of the ERBE results with general circulation models (GCMs) show that global net cloud forcing can be determined reasonably well from some current versions of the GCMs. Modeled regional and zonal values of radiative cloud forcing, however, indicate a need for considerable improvement.

INTRODUCTION

Cloudiness is a pivotal variable for the balance of Earth's radiant energy. Clouds reflect incoming solar (shortwave) radiation, increasing the planetary albedo significantly above the clear-sky value. This effect serves to cool the Earth-atmosphere system. On the other hand, clouds absorb longwave radiation emitted at relatively high temperatures by the Earth's surface. They then reradiate to space at lower temperatures, which depend on cloud height and optical thickness. The reduction of the longwave flux to space by clouds produces a net heating of the Earth-atmosphere system. This is commonly referred to as the greenhouse effect. Thus clouds have two competing effects on Earth's radiation balance. As a result, there is a key climatic question of whether clouds, on the average, increase or decrease the Earth's net radiation.

Numerous studies [see *Hartmann et al.*, 1986] have addressed this question both observationally [e.g., *Cess*, 1976; *Ohring and Clapp*, 1980] and theoretically [e.g., *Somerville and Remer*, 1984; *Charlock and Ramanathan*, 1985]. Except for a few limited studies [e.g., *Minnis and Harrison*, 1984], the accuracy of most observational results concerning climate-scale cloud radiative effects has been diminished by the data available to define clear-sky and total radiation fields. The difficulties of determining the overall cloud effects on the global radiation budget with general circulation models (GCMs), summarized by *Cess and Potter* [1987], also lead to relatively large uncertainties in the answer.

The Earth Radiation Budget Experiment (ERBE); [see *Barkstrom*, 1984] is the first satellite experiment designed to provide observational data to address this important climatic problem. Initial results from the ERBE for April 1985 [*Ramanathan et al.*, 1989] have shown that clouds produce a net cooling of the Earth-atmosphere system. With the availability of additional ERBE data, it is now possible to study the effects of clouds on the radiation budget for all seasons. This paper documents the seasonal variations of cloud-radiation effects using the ERBE data. The results are discussed in terms of their potential impact on the climate and compared to published values of corresponding parameters from various GCM calculations.

DATA

The data used here consist of top-of-the-atmosphere, monthly mean shortwave (0.2–5.0 μm), albedo α, and outgoing longwave (5.0–50.0 μm) flux F. The values are derived from radiances measured by the ERBE scanners [*Kopia*, 1986] on the Earth Radiation Budget Satellite (ERBS) and NOAA 9 spacecraft. The ERBE data processing system produces both clear-sky and total radiative parameters on a 2.5° grid. (For details of the processing, see *Barkstrom and Smith* [1986], *Smith et al.* [1986], *Brooks et al.* [1986], and *Suttles et al.* [1988, 1989].) A maximum likelihood estimator technique [*Wielicki and Green*, 1989] is used to categorize each measurement in terms of percent cloudiness: clear

[1]Atmospheric Sciences Division, NASA Langley Research Center, Hampton, Virginia.
[2]Department of Geophysical Sciences, University of Chicago, Illinois.
[3]Laboratory for Planetary and Atmospheric Research, State University of New York at Stony Brook.
[4]Lockheed Engineering and Sciences Company, Hampton, Virginia.

Paper number 90JD01215.
0148-0227/90/90JD-01215$05.00

(0–5%), partly cloudy (5–50%), mostly cloudy (50–95%), and overcast (95–100%). (A description of the archived ERBE data products, and a discussion of the ERBE instruments, data processing, and validation is given by *Barkstrom et al.* [1989]. The ERBE data are available to the scientific community through the National Space Science Data Center (NSSDC). Within the United States, the address is National Space Science Data Center, Code 633.4, Goddard Space Flight Center, Greenbelt, Maryland 20771. For scientists outside the United States, the address is World Data Center A, Rockets and Satellites, Code 630.2, Goddard Space Flight Center, Greenbelt, Maryland 20771, USA.)

Mean clear-sky parameters, computed from all measurements identified as clear, are assumed to represent the average fields for cloud-free scenes and are denoted with the subscript clr. Mean total parameters include all data regardless of scene identification. Examples and preliminary validation of the longwave (LW) data products for April 1985 were presented by *Harrison et al.* [1988]. The current study uses averages derived for the months of April, July, and October 1985 and January 1986. These months represent the four seasons.

CLOUD-RADIATIVE FORCING

The effects of clouds on the Earth's radiation balance are examined here in terms of the difference between the clear-sky and the total-scene radiation results. This difference is defined as cloud-radiative forcing [*Charlock and Ramanathan*, 1985; *Hartmann et al.*, 1986; *Ramanathan*, 1987; *Cess and Potter*, 1987; *Ramanathan et al.*, 1989]. Thus cloud-radiative forcing for LW flux is

$$C_{LW} = F_{clr} - F$$

and cloud-radiative forcing for shortwave (SW) flux is

$$C_{SW} = S(\alpha_{clr} - \alpha)$$

where S is the monthly mean incoming solar flux for the region. Net cloud-radiative forcing is

$$C = C_{LW} + C_{SW}$$

These three cloud-forcing parameters are important diagnostic indexes of the impact of clouds on radiation. They can be easily computed from any data set which explicitly contains both total and clear-sky fluxes.

ERBE RESULTS

Regional results are presented for July 1985 and January 1986. These 2 months are near the summer and winter solstices, respectively, and encompass the seasonal extremes of radiation. Zonal means for the 4 months are shown to examine seasonal variations of the various radiative parameters.

Regional Measurements

Clear-sky and total albedos are shown in Plates 1*a* and 1*b* for July and Plates 1*c* and 1*d* for January, respectively. Clear-sky and total LW fluxes are given in Plate 2. Results are shown in color on a Hammer-Aitoff projection, which provides an elliptical, equal-area representation of the entire Earth and also minimizes distortion of continent shapes. Latitudes are indicated every 30° and longitudes every 90°.

The clear-sky albedos outline the major surface features in both months (Plates 1*a* and 1*c*). The color palette was selected to facilitate easy interpretation of the data. In general, a single color represents a 12% albedo range. Exceptions are made at the lower end of the scale to permit enhancement of features of particular interest, such as the minimum observed albedo (about 9%), slight albedo variations over oceans due to a solar zenith angle effect, and the transition between ocean and land, which occurs at an albedo of about 15%. Gray indicates that no clear-sky data were available for the month. Whenever appropriate, isolated regions having no clear-sky measurements were filled by interpolation using data from adjacent regions having the same type of surface background. The hard color boundaries on the plots provide the same data as a traditional contour plot, but the color fill makes significant features easier to discern.

High albedo ($\alpha_{clr} > 36\%$) areas poleward of 40°N during January correspond primarily to snow- and ice-covered regions. Satellite-derived maps of snow cover were obtained from the National Environmental Satellite Service of NOAA [see *Dewey*, 1987] and incorporated into the ERBE data analysis systems. Mountainous areas, such as the western United States, with variable snow cover have clear-sky albedos which are closer to those having only vegetation ($\alpha_{clr} \sim 25\%$). Desert areas in north Africa and Saudi Arabia are substantially brighter than surrounding regions during both months. Tropical forests in South America and Africa have low albedos (~15%). Oceanic regions have the lowest clear-sky albedos (<15%). The increase in ocean clear-sky albedo near the wintertime pole reflects the effects of the high solar zenith angles at those latitudes [*Briegleb et al.*, 1986].

Longwave fluxes are shown in Plate 2. The warmer end of the scale uses more colors in order to better display significant features in the tropics. As before, the color boundaries can be used to provide quantitative "contour plot" information. Clear-sky LW fluxes range from ~100 W m^{-2} over Antarctica to ~330 W m^{-2} over the Middle East during July. The range is reduced by ~70 W m^{-2} in January (Plate 2*c*), when a minimum clear-sky LW flux of ~150 W m^{-2} is found over Greenland and a maximum of ~310 W m^{-2} is observed over Australia. Highlands and areas of high humidity (e.g., rain forests) appear cooler than surrounding regions at the same latitudes. Northeastward penetration of the Gulf Stream is apparent in the clear-sky LW flux pattern in January.

The total albedo and LW flux patterns reveal the combined effects of clouds and clear skies. For example, total albedo over north Africa is relatively constant at ~35% during July (Plate 1*b*), although the southern half of the region is nearly overcast and the northern half is clear. The effects of clouds over Africa become more apparent during January (Plate 1*d*), when the intertropical convergence zone (ITCZ) moves southward, exposing the darker surfaces of the Sahel and central Africa. Marine stratus and stratocumulus west of the continents in the subtropics have albedos substantially higher than the underlying surface, but the presence of these low-altitude clouds is not as evident in the LW fluxes (Plate 2).

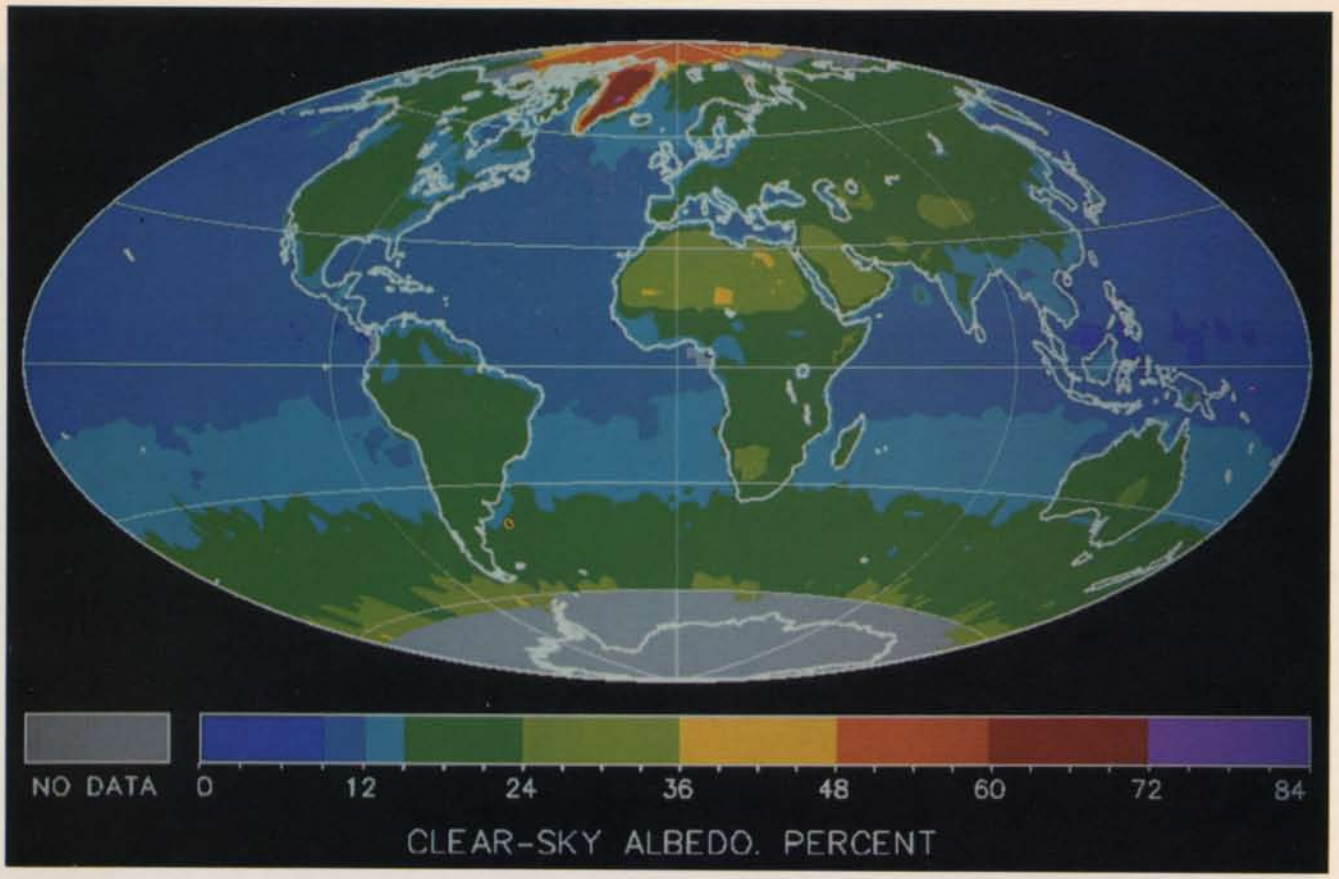

Plate 1*a*

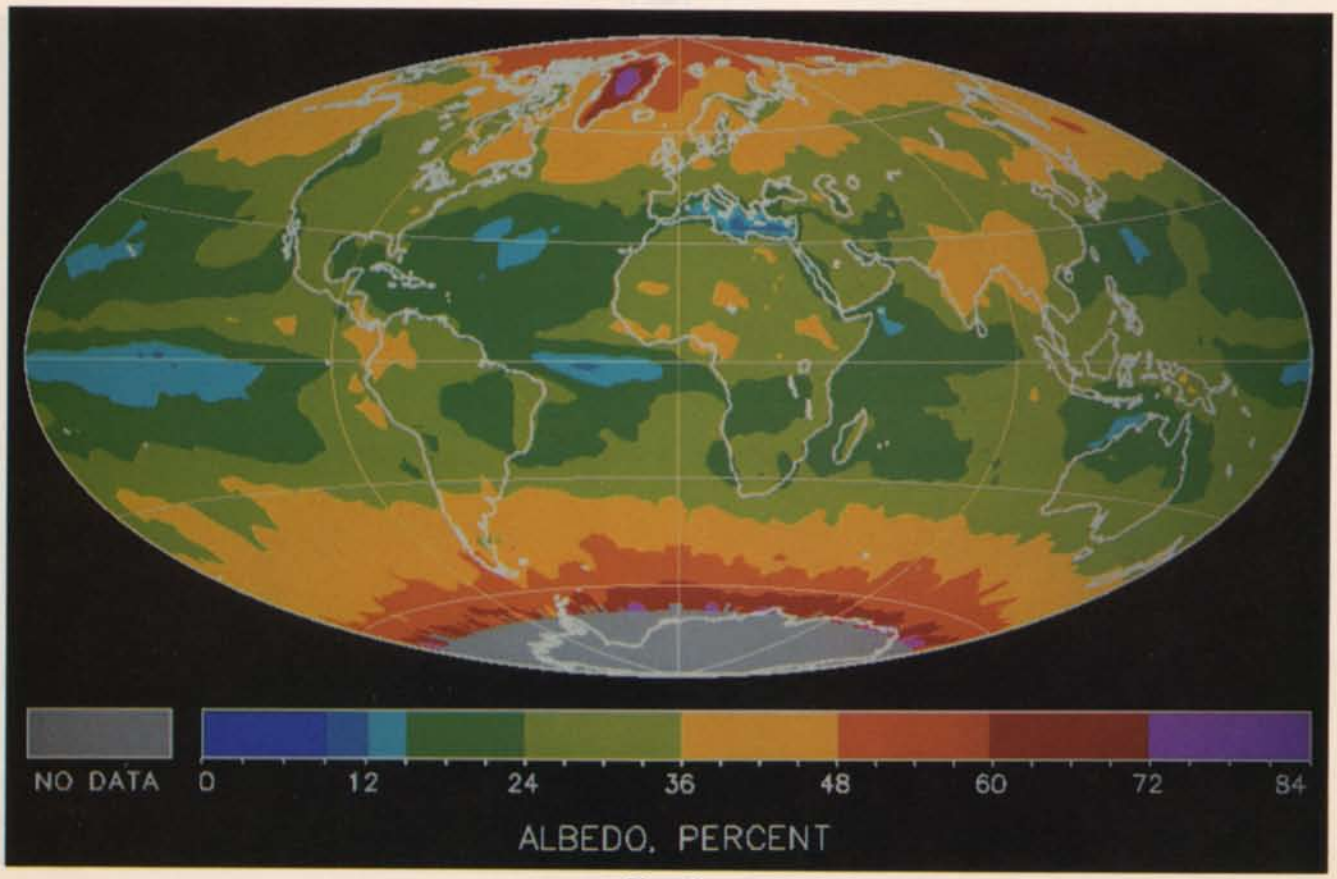

Plate 1*b*

Plate 1. ERBE monthly mean (*a*) clear-sky and (*b*) total albedo for July 1985, and (*c*) clear-sky and (*d*) total albedo for January 1986.

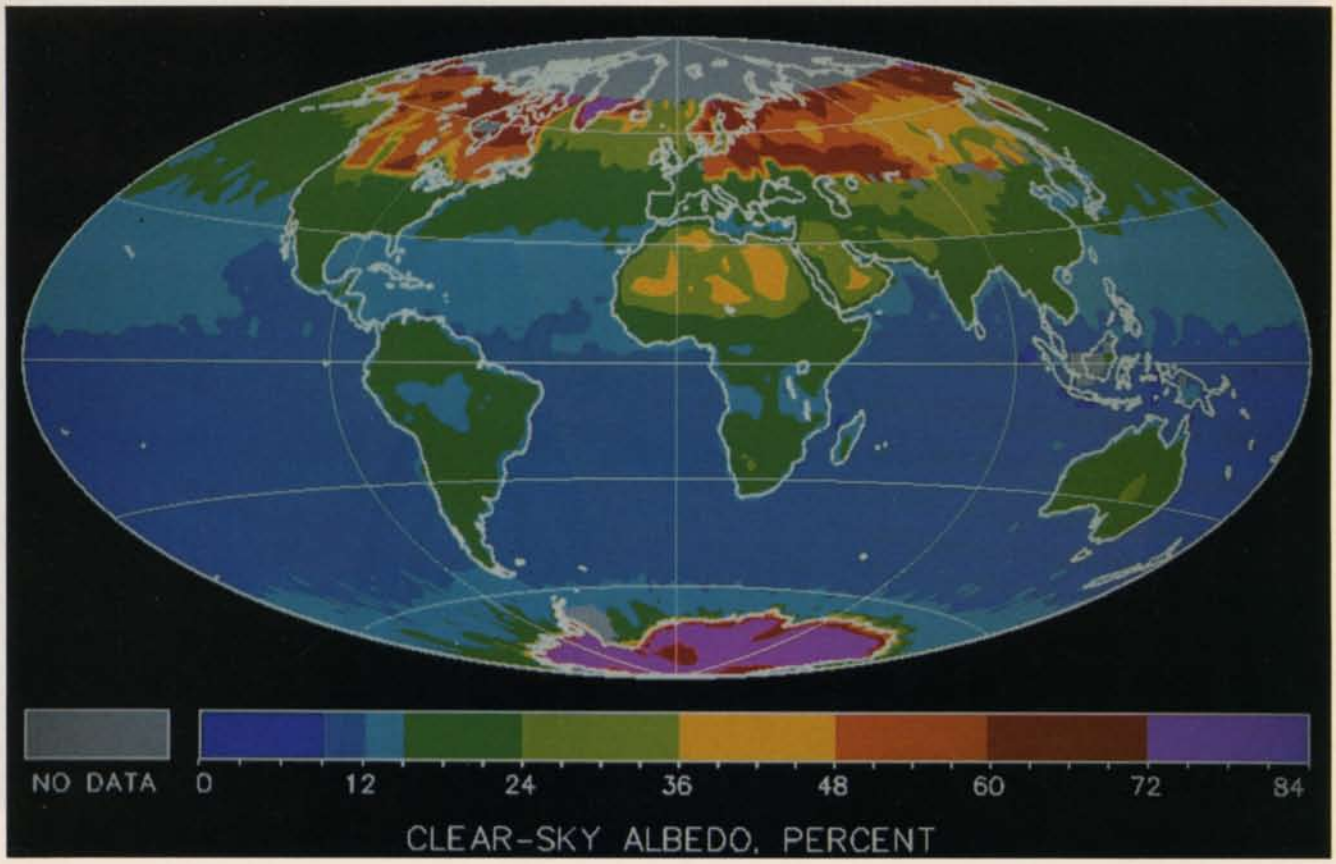

Plate 1*c*

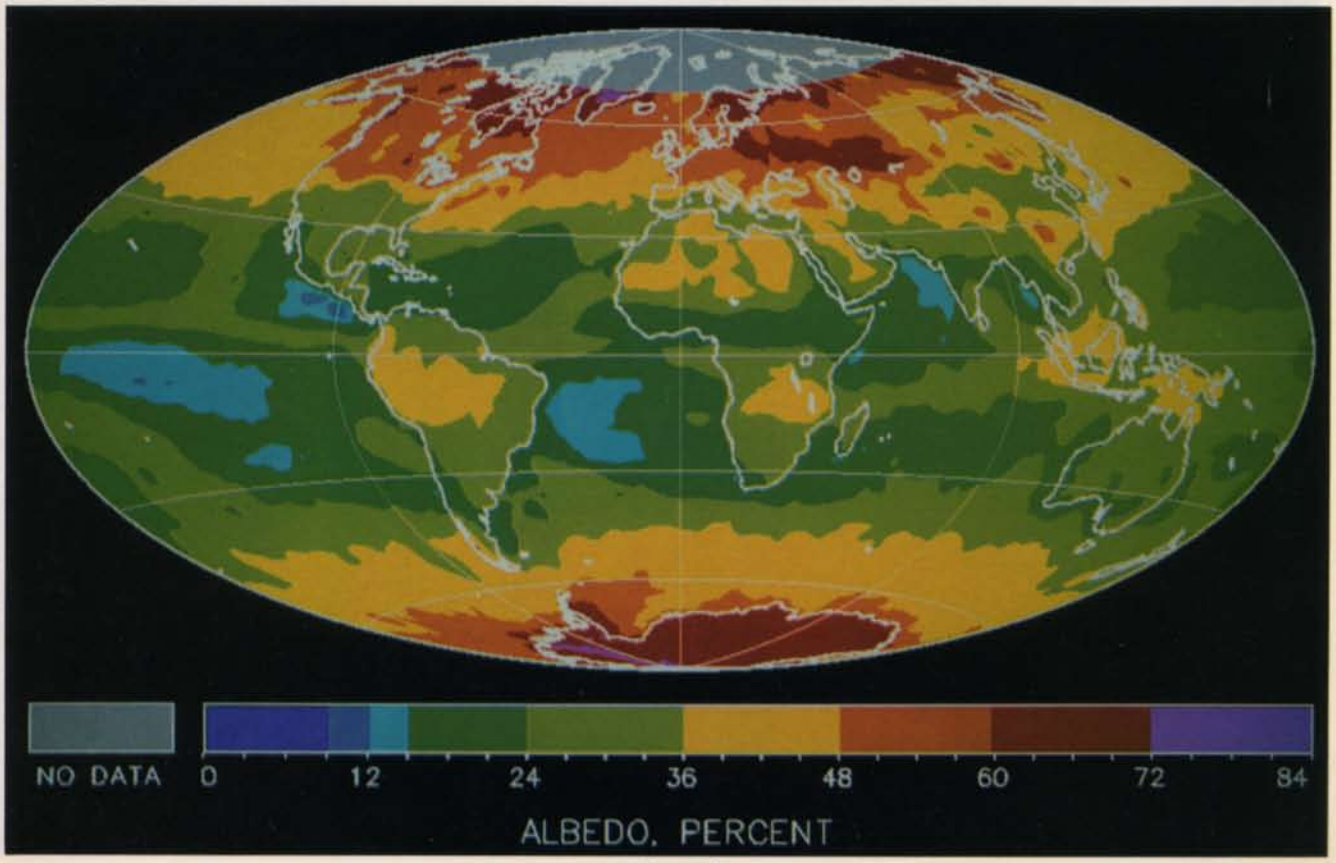

Plate 1*d*

Plate 1. (continued)

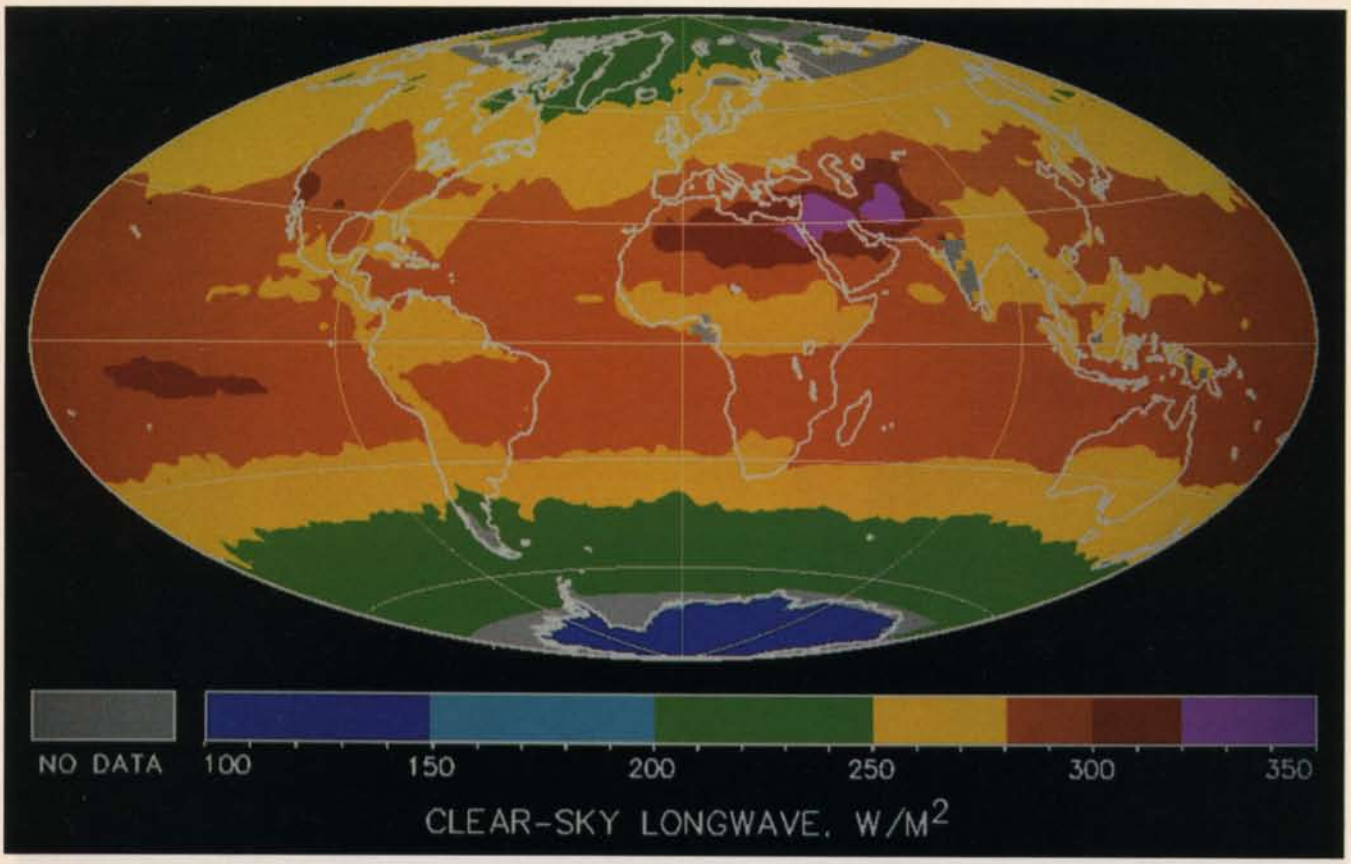

Plate 2*a*

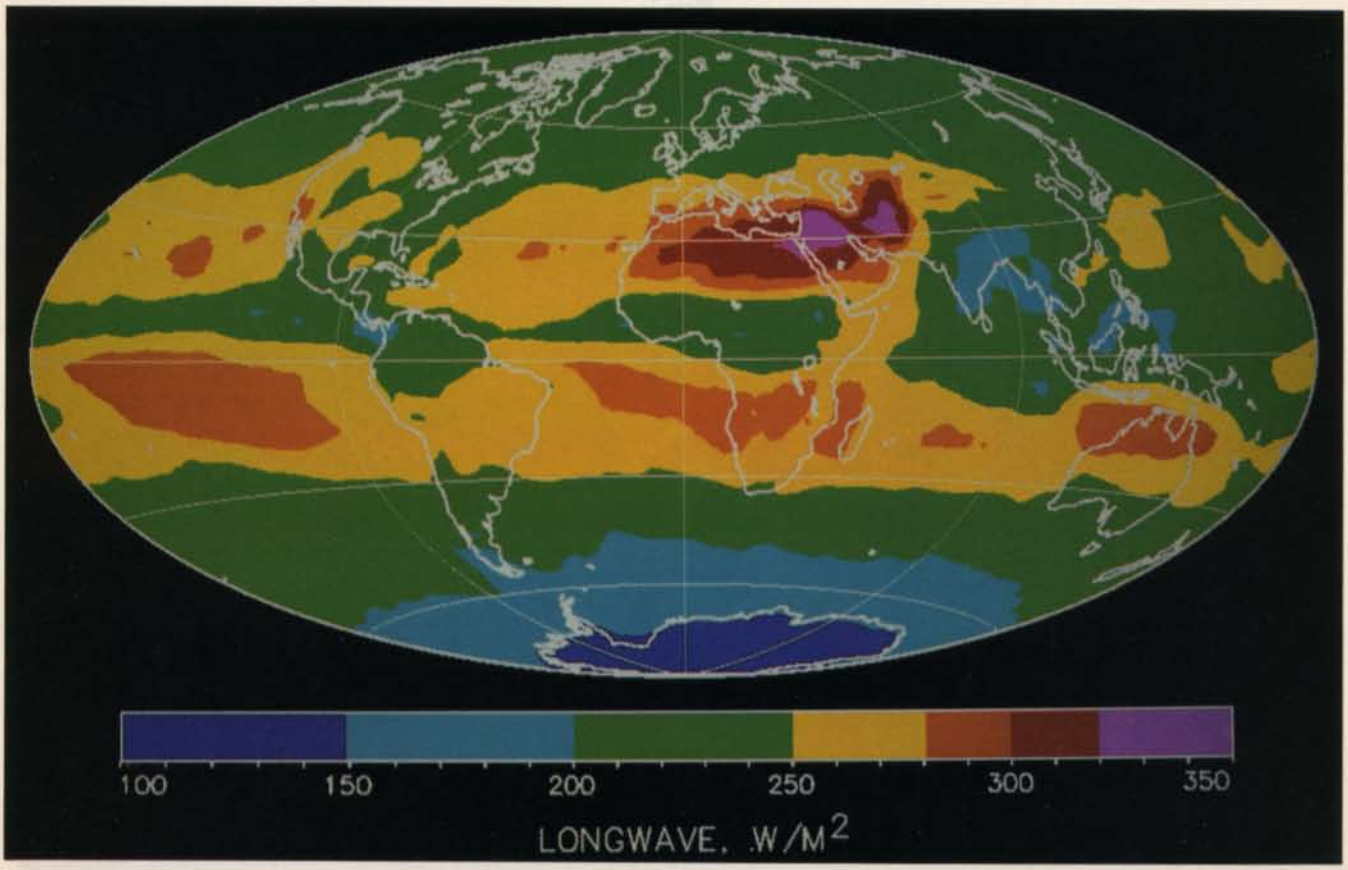

Plate 2*b*

Plate 2. ERBE monthly mean (*a*) clear-sky and (*b*) total LW flux for July 1985, and (*c*) clear-sky and (*d*) total LW flux for January 1986.

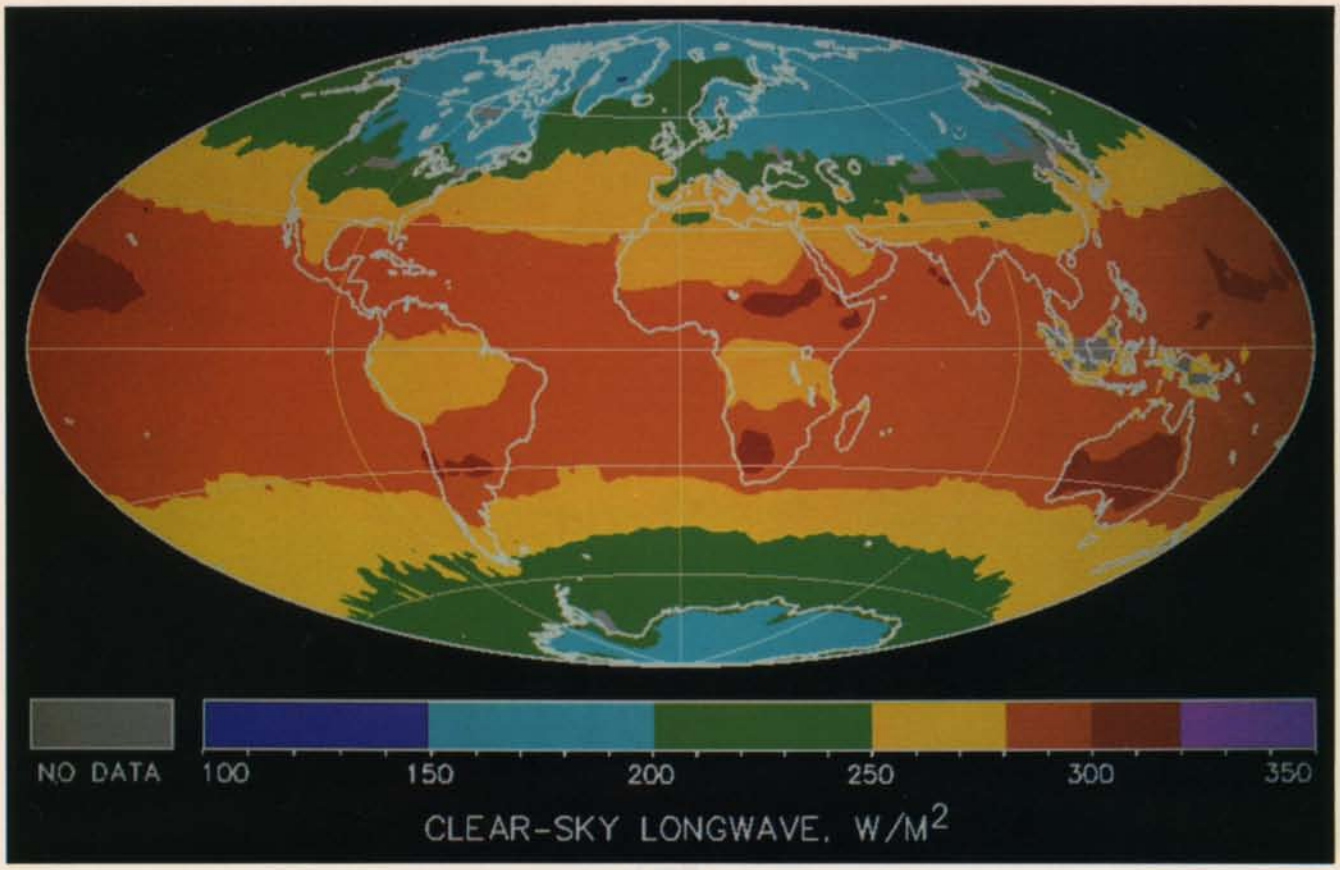

Plate 2*c*

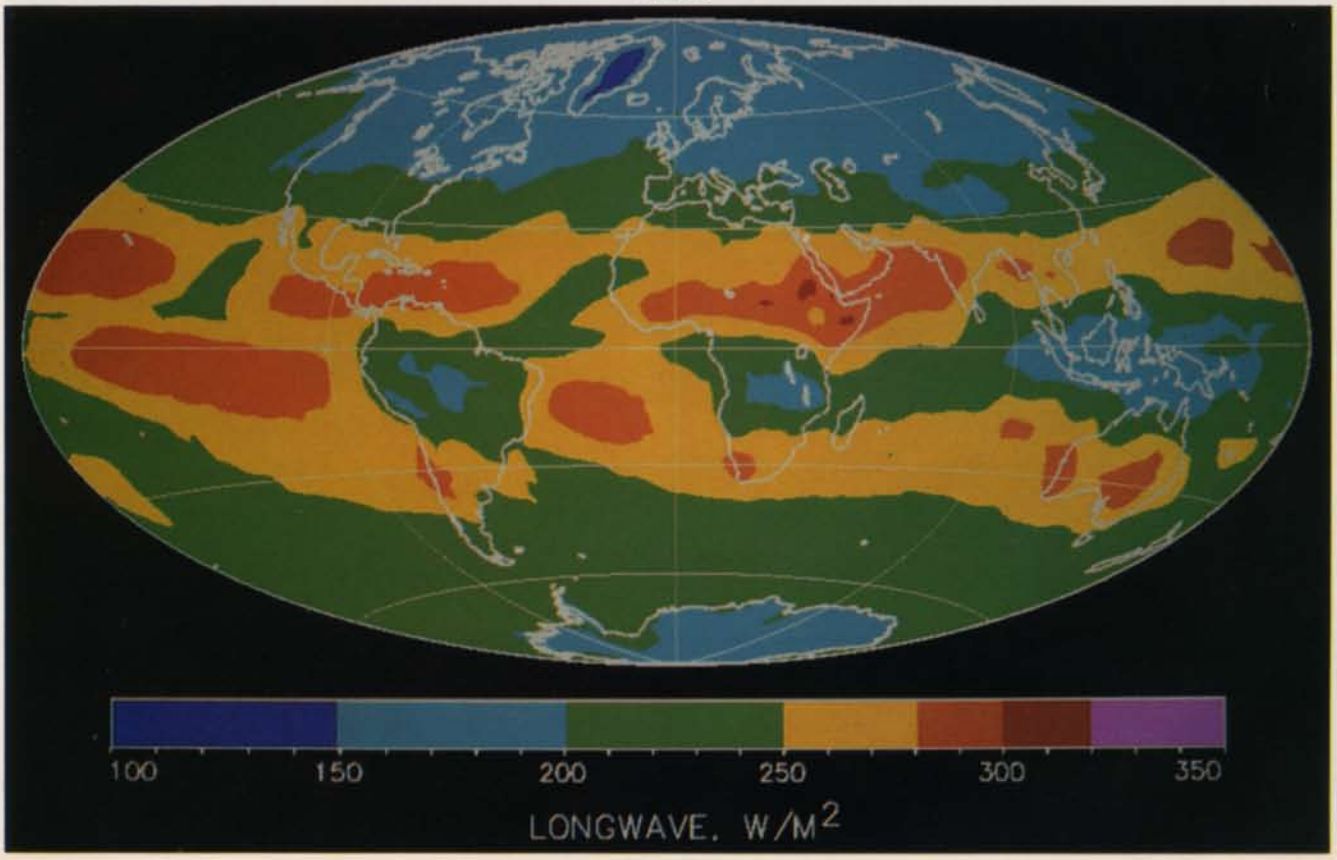

Plate 2*d*

Plate 2. (continued)

Regional Cloud Forcing

The global distribution of C_{LW} derived from the ERBE for July 1985 is presented in Plate 3*a*. In this plot, each color represents a range of 20 W m^{-2}. Peak values are found over northern tropical regions such as Central America, Congo Basin, and Indonesia, where deep convective clouds are prominent. These high-altitude clouds reduce the LW emission to space by 60–100 W m^{-2}. Other regions with significant longwave cloud forcing (20–60 W m^{-2}) are associated with the mid-latitude storm tracks over the Pacific and Atlantic oceans in both hemispheres. Optically thick, high clouds, with their associated cold cloud-top temperatures, reduce the emission more than low clouds. Small values of C_{LW} correspond to areas which may be characterized by various combinations of clear skies, low clouds, optically thin clouds, or cold surfaces.

The southerly shift of the ITCZ and the intensification of the mid-latitude storm tracks from July to January are evident in the distribution of C_{LW} for the 2 months (Plate 3). Maximum values of C_{LW} are greater over the northern mid-latitudes during January than they are over the southern mid-latitudes during the austral winter. Longwave cloud forcing appears to be relatively insensitive to season over the Sahara Desert. The largest values of C_{LW} found over the tropical regions and the mid-latitude storm tracks for July (Plate 3*a*) are similar to those determined for April 1985 [*Ramanathan et al.*, 1989]. In the North Atlantic during January, the LW cloud forcing is most intense near the coast of North America, where cool continental air flows over the relatively warm ocean. This maximum, which is much greater during January than during July, tends to follow the Gulf Stream toward Europe.

The LW cloud forcing results in Plates 3*a* and 3*b* may be compared with the distributions of C_{SW} obtained from ERBE for July and January in Plates 4*a* and 4*b*, respectively. In the tropics during July, maximum negative values occur over Central America and ocean regions off the western coast of this area, near the western coast of Africa at about 10°N, in the Indian monsoon regions, and over a large region near the Philippines centered at 8°N, 120°E. During January, maximum shortwave cloud cooling occurs over central South America and in areas within the ITCZ starting in Africa at 8°S, 40°E and extending along a line eastward through New Guinea to about 10°S, 140°E. The SW cloud forcing over the ITCZ areas is almost equal in magnitude, but opposite in sign to C_{LW}. Negligible SW cloud forcing occurs over north Africa and the Arabian Peninsula during both months and, during July, over the southern hemisphere deserts. These small values are primarily due to the lack of any substantial cloudiness over those areas [see *Hwang et al.*, 1988]. Any small positive values are generally associated with snow-covered regions and are within the uncertainty range of the observations. The most striking difference between C_{LW} and C_{SW} is seen in the mid-latitudes. The SW cloud forcing has a maximum magnitude of -140 W m^{-2} at 60°S in January and between 50°N and 70°N over the oceans in July. For comparison, C_{LW} is less than 40 W m^{-2} at these latitudes during both months.

The global patterns of C_{LW} and C_{SW} reflect the major climatic regimes and organized cloud systems of the Earth. As noted earlier, distinguishing between clear and cloudy scenes over bright ice- and snow-covered regions is extremely difficult. Hence the cloud forcing results in the vicinity of the Arctic and Antarctic should be used with considerable caution. It will be shown later, however, that these polar regions contribute little to the global cloud forcing.

The global distribution of net cloud radiative forcing is depicted in Plates 5*a* and 5*b* for July and January, respectively. In the tropics, the LW and SW cloud forcing nearly cancel over many areas. This is expected over areas such as the central Pacific, western Atlantic, deserts, and the Arabian Sea, where little cloudiness is found. Some areas on the fringes of the ITCZ also have small values of C. The net forcing there is within the estimated uncertainty in the measurements of regional cloud radiative forcing. Negative net cloud forcing in the tropics occurs primarily over the marine stratus systems near the eastern edges of the oceans and over the centers of the areas of strongest convective activity in southeastern Asia, central America, and sub-Sahelian Africa during July and in northern South America, southern Africa, and the Arafura Sea during January. Positive cloud forcing in the tropics is adjacent to the significant areas of deep convection. During January, the largest area with positive cloud forcing is found in the western Pacific, at ~10°N away from the core of the Indonesian/New Guinea convergence area. The positive area shifts to the south as the southeast Asia monsoon is established in July. During July, the cloud forcing is also positive near the Sahara-Sahel boundary in Africa.

The largest negative cloud forcing is found over the storm tracks at middle to high (45°–70°) latitudes in the summer hemisphere, where the cloud albedo effects outweigh the greenhouse effects. Similarly, the largest positive values of C follow the storm tracks in the winter hemisphere between 50°S and 70°S during July and between 45°N and 70°N during January. The most extreme values occur over marine areas, since the contrast in albedo between clear and cloudy conditions is greatest over oceans.

Zonal Cloud Forcing

The latitudinal variations of C_{LW}, C_{SW}, and C are presented in Figures 1*a*, 1*b*, and 1*c*, respectively, for all 4 months. Longwave cloud forcing exhibits a relatively small range (10–50 W m^{-2}) of latitudinal and seasonal changes in comparison to C_{SW}, which varies significantly from 0 to -150 W m^{-2}. Gradually, at a given latitude the cloud forcing variations are bounded by the values for winter and summer seasons. The maximum fluctuation in C_{LW} occurs in the tropics, whereas C_{SW} and C vary most at the middle and high latitudes. The equator-to-pole gradient is largest in the summer hemisphere.

A summary of global values of clear-sky and total-scene LW and absorbed SW along with the radiative cloud forcing results is given in Table 1 for the four seasons. Generally, there is a small seasonal effect on the global values of these parameters. The global annual SW cloud forcing is -48 W m^{-2}. Mean global LW cloud forcing is 31 W m^{-2}, resulting in a net cloud forcing of -17 W m^{-2}. April has the minimum net cloud forcing magnitude of -14 W m^{-2}, and January has the maximum value of -21 W m^{-2}. The variation of cloud forcing between hemispheres is significant during winter and summer months, as shown in Table 2. Longwave and SW cloud forcing terms nearly cancel each other in the winter

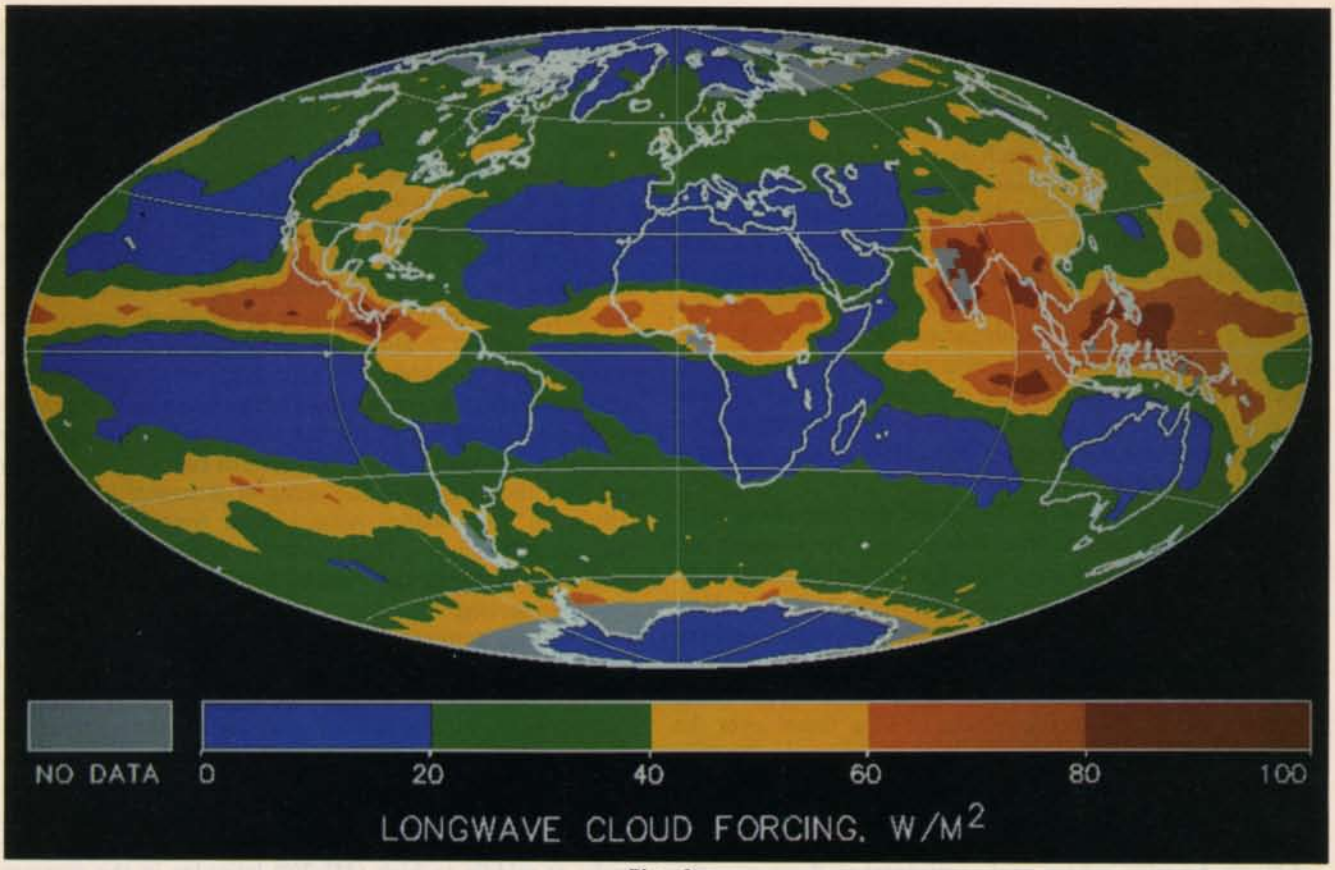

Plate 3*a*

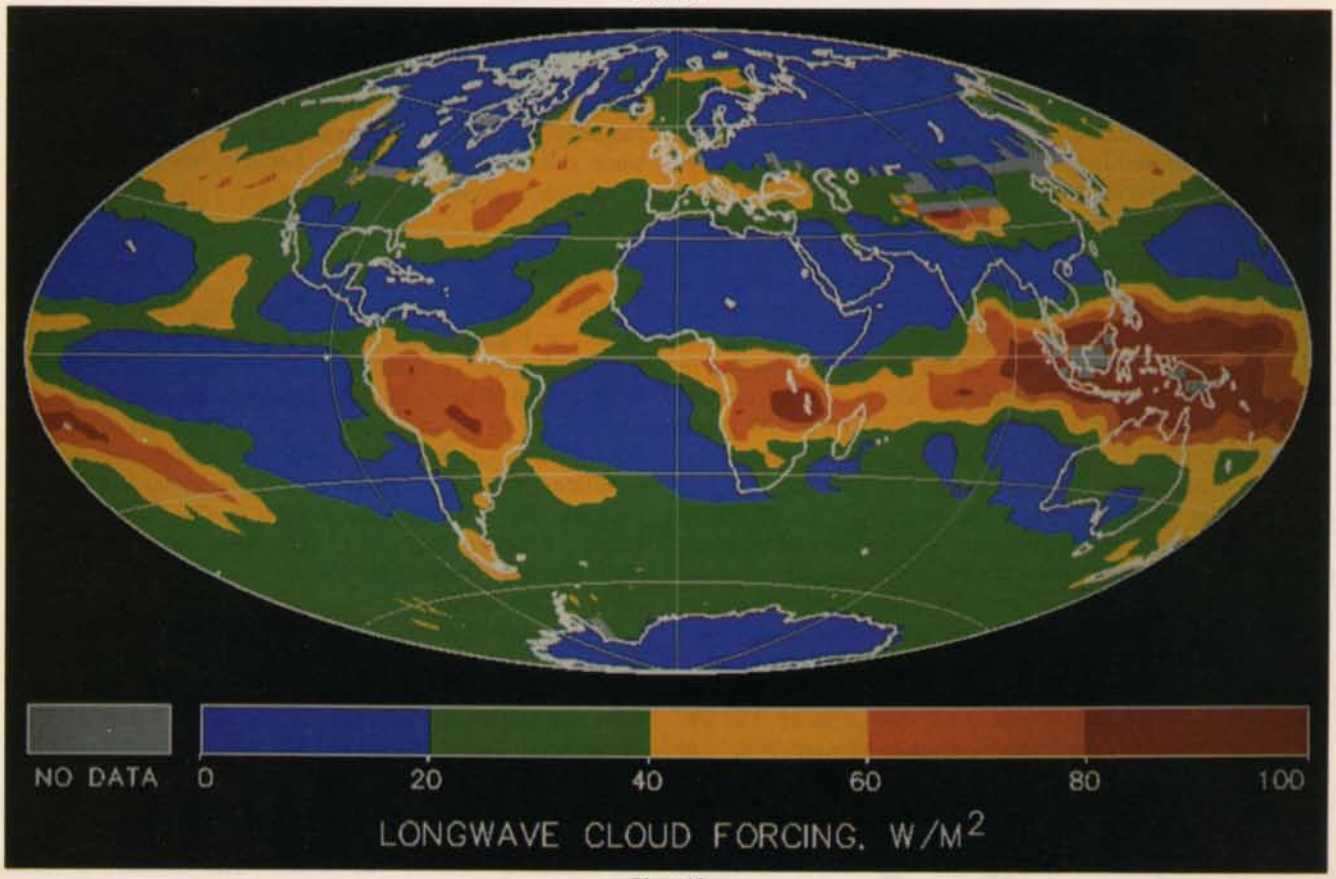

Plate 3*b*

Plate 3. LW cloud radiative forcing from ERBE for (*a*) July 1985 and (*b*) January 1986.

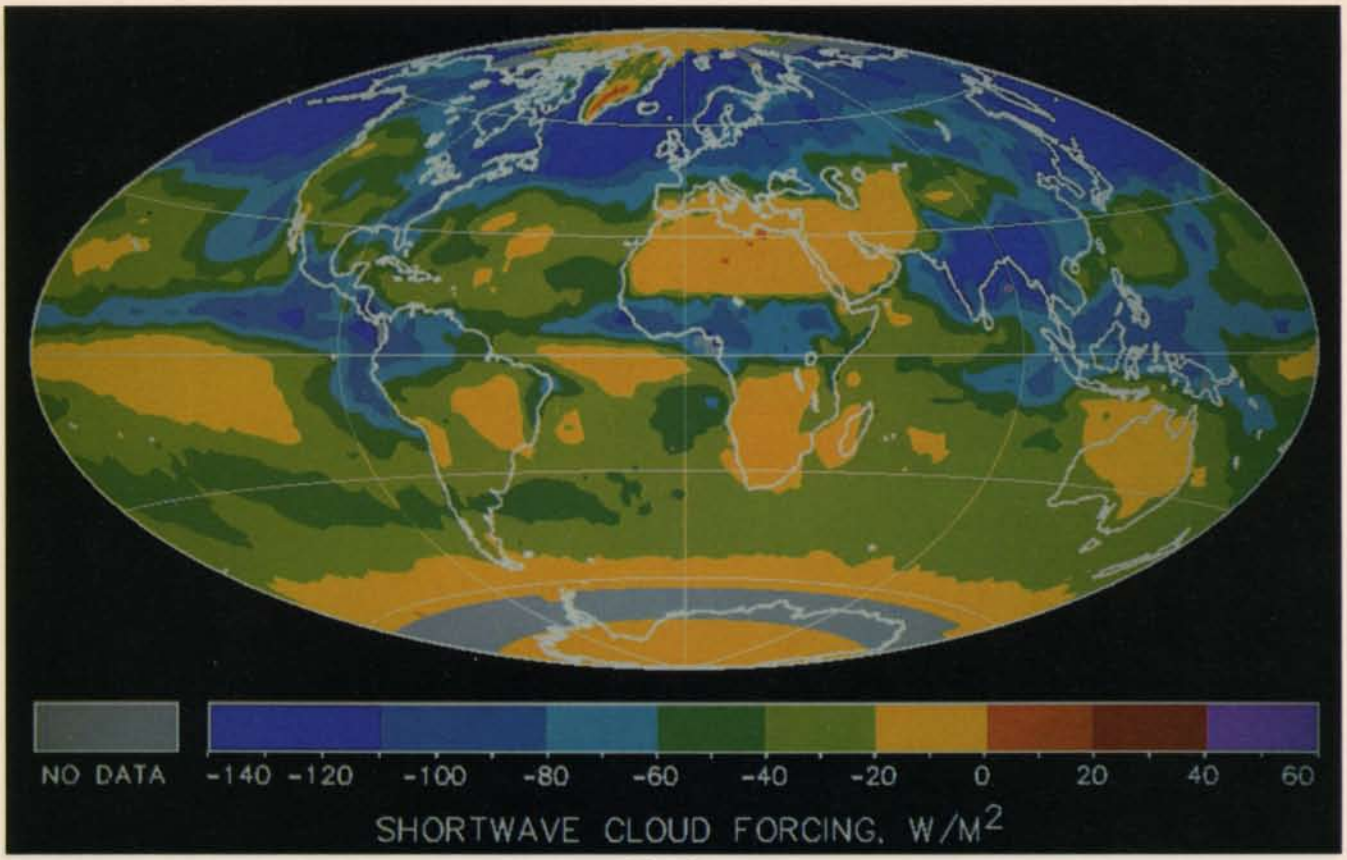

Plate 4*a*

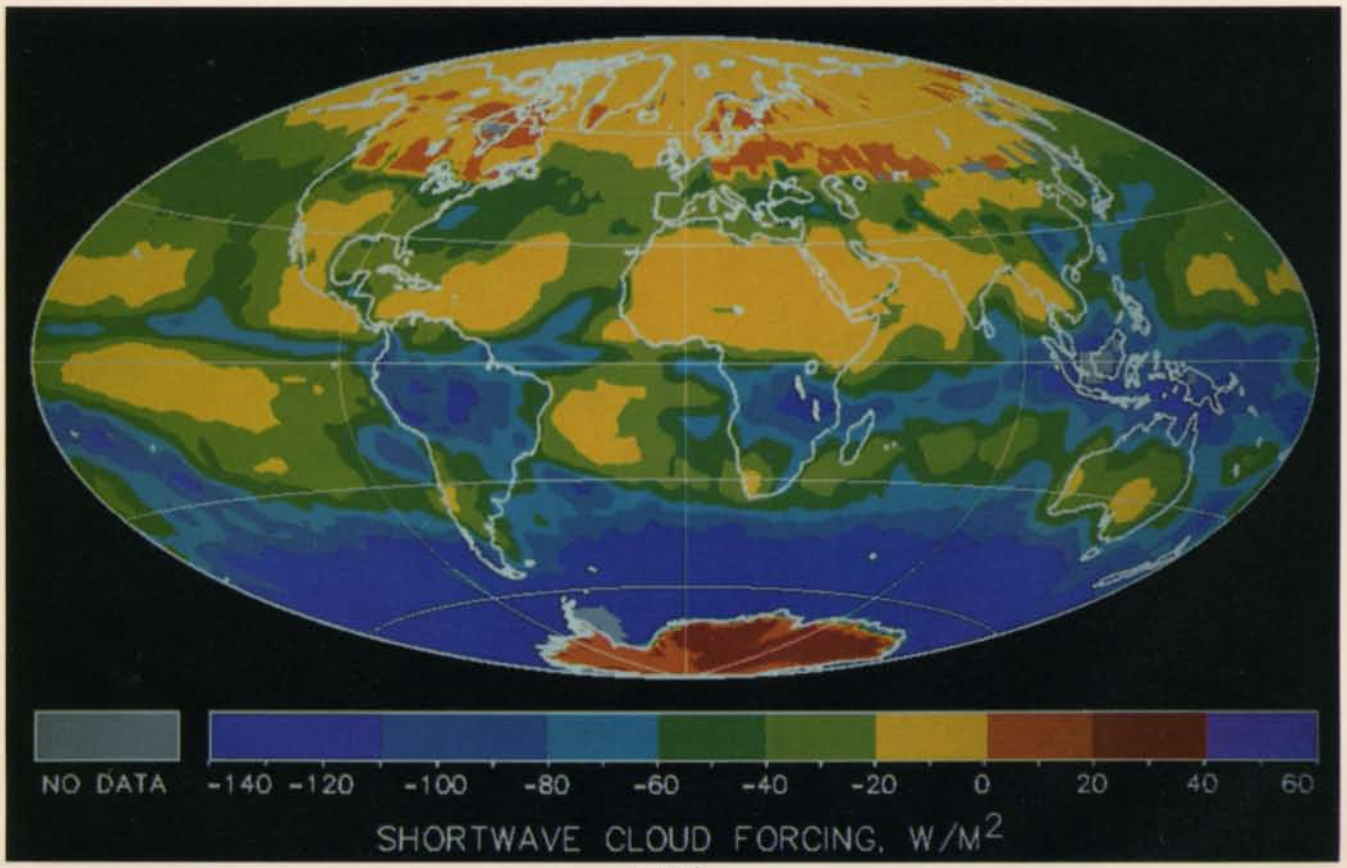

Plate 4*b*

Plate 4. SW cloud radiative forcing from ERBE for (*a*) July 1985 and (*b*) January 1986.

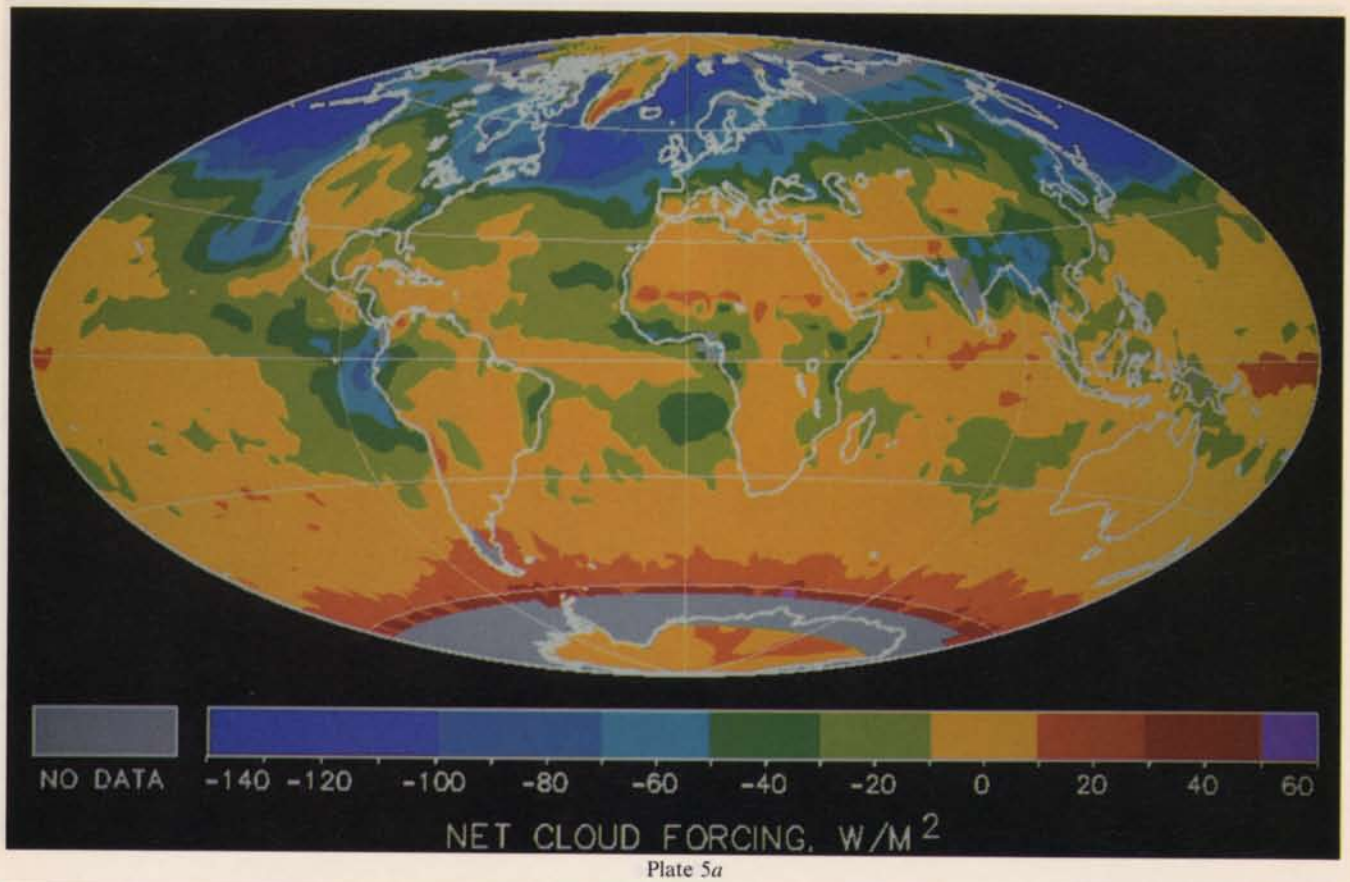

Plate 5*a*

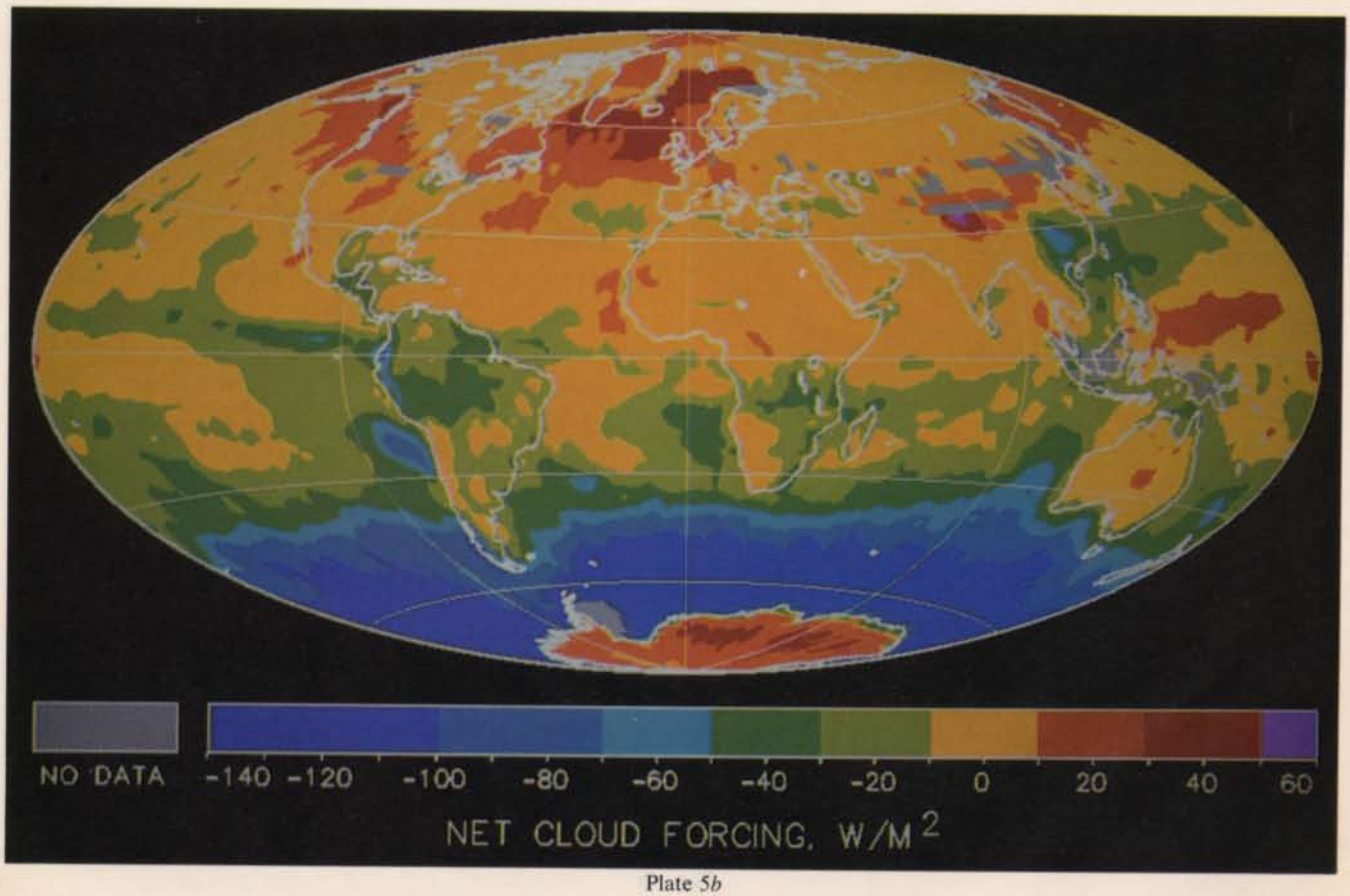

Plate 5*b*

Plate 5. Net cloud radiative forcing from ERBE for (*a*) July 1985 and (*b*) January 1986.

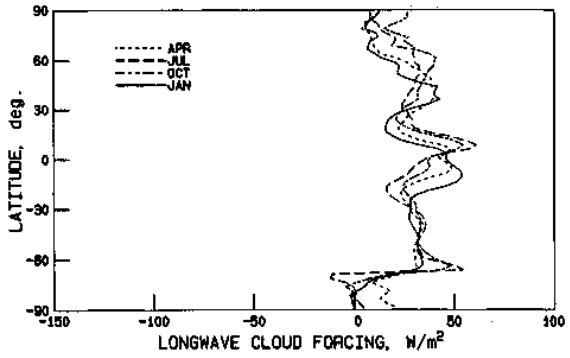

Fig. 1*a*

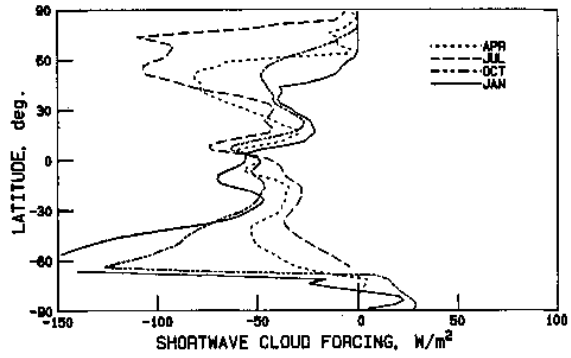

Fig. 1*b*

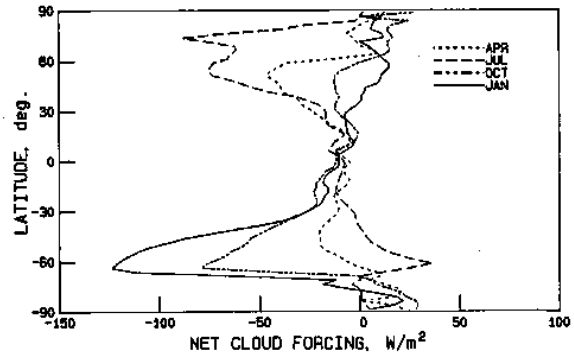

Fig. 1*c*

Fig. 1. Latitudinal variation of (*a*) LW, (*b*) SW, and (*c*) net cloud radiative forcing from ERBE for April, July, and October 1985 and January 1986.

hemisphere. Shortwave forcing is twice as large (but of opposite sign) as the LW positive forcing in the summer hemisphere. As a result, the net cloud forcing is either near zero or negative in each hemisphere, and the global value is negative. For the spring and fall seasons, both hemispheres have negative net cloud forcing. Therefore, globally, clouds have more of an albedo or cooling effect than a greenhouse heating effect on net radiation for all seasons.

Snow and Ice Contributions

ERBE identifies snow-covered scenes as either clear or overcast. Since the scene identification algorithm over snow is considered highly unreliable, the value of C over snow is also suspect. Given that the ERBE scene identification scheme cannot reliably distinguish between clear and overcast over snow, it is reasonable to assume that cloud forcing over snow-covered regions is small. Therefore, in order to avoid biasing the global averages by using the questionable cloud forcing results over snow, it was assumed that $C_{LW} = C_{SW} = C = 0$ over the snow regions. The maximum effect of this assumption occurs in April, where a net decrease of 2 W m^{-2} in the global value of C was calculated using zero cloud forcing over snow instead of the results from ERBE processing. A summary of the results for all four months is presented in Table 3. In this table, ΔCF represents the change in the global cloud forcing parameter due to the assumption of zero cloud forcing over snow-covered regions. The maximum effect occurs in April with a net decrease of 2 W m^{-2} in C. The annual average C decreases by 5% if snow-covered regions are assumed to be clear in the analysis. This result is consistent with a small positive value of C over snow areas as expected from the input to the ERBE scene classification algorithm [*Suttles et al.*, 1988, 1989]. Thus it is concluded that scene identification errors over snow do not introduce significant errors in the global values of cloud forcing.

The minimal effect of the snow-covered regions on global cloud forcing is also supported by GCM results. In a perpetual January GCM simulation, *Charlock and Ramanathan* [1985] found that C_{SW} was near zero over the Antarctic continent because clouds have little additional reflective effect over snow and ice. Also, the polar regions exhibited minimum values of C_{LW} because the temperature difference between the surface and the cloud top is small there; in high latitudes, both the cloud altitudes and the atmospheric lapse rates are lower. These general findings were also supported by results from other GCM simulations reported by *Cess and Potter* [1987]. For the ERBE January case in Table 3, substitution of cloud forcing over snow obtained from GCM results ($C_{SW} = -5$ W m^{-2}, $C_{LW} = 20$ W m^{-2}) would yield less than a 2 W m^{-2} decrease in the global value of C_{SW}, a similar increase in C_{LW}, and almost no difference in net cloud forcing.

Uncertainties

Although a complete, rigorous error analysis of all of the ERBE products is not yet available, several studies have

TABLE 1. Summary of Cloud Radiative Forcing Parameters (W/m²)

Date	Longwave	Clear-Sky Longwave	Longwave Cloud Forcing	Shortwave Absorbed	Clear-Sky Shortwave Absorbed	Shortwave Cloud Forcing	Net Cloud Forcing
April 1985	234.5	265.8	31.3	236.5	281.6	−45.1	−13.8
July 1985	237.5	267.6	30.1	234.4	281.1	−46.7	−16.6
Oct. 1985	234.1	266.3	32.2	243.0	293.1	−50.1	−17.9
Jan. 1986	231.9	262.5	30.6	243.3	295.0	−51.7	−21.1
Annual	234.5	265.6	31.1	239.3	287.7	−48.4	−17.3

TABLE 2. Hemispheric Differences in Seasonal Cloud Forcing

Date	Geographical Extent	Cloud Forcing		
		LW	SW	Net
April 1985	Northern hemisphere	31.2	−49.8	−18.6
	Southern hemisphere	31.5	−40.4	−8.9
	Global	31.3	−45.1	−13.8
July 1985	Northern hemisphere	33.8	−66.3	−32.5
	Southern hemisphere	26.4	−27.2	−0.8
	Global	30.1	−46.7	−16.6
Oct. 1985	Northern hemisphere	34.1	−40.1	−6.0
	Southern hemisphere	30.2	−60.2	−30.0
	Global	32.2	−50.1	−17.9
Jan. 1986	Northern hemisphere	26.6	−26.7	−0.1
	Southern hemisphere	34.7	−76.8	−42.1
	Global	30.6	−51.7	−21.1
Annual	Northern hemisphere	31.4	−45.7	−14.3
	Southern hemisphere	30.7	−51.1	−20.4
	Global	31.1	−48.4	−17.3

already examined some of the sources for error in the ERBE data. The most significant errors arise from misclassifications of particular scene types and from sampling deficiencies. Scene identification errors result in the selection of the wrong anisotropic models and the incorrect categorization of a given measurement. The anisotropic models also have some inherent uncertainties which may not be entirely eliminated through averaging. Incorrect categorization may result in biases in the average fluxes for a given scene type. Sampling errors result from variations in meteorology and optical properties not taken into account in the procedures which compute monthly average fluxes from measurements taken at four or five times during each day.

Using a limited set of correlative data, *Diekmann and Smith* [1989] evaluated the effects of scene identification errors on total instantaneous flux estimates. They reported that the longwave error is generally negligible and the average standard deviations of shortwave flux can reach maximum values of more than 13% of the exitance value. The highest errors were found for partly and mostly cloudy ocean scenes. ERBE identification of clear and overcast scenes is very reliable with errors generally less than 2%. Assuming that every fifth pixel is statistically independent, the averaging over space and time for a 2.5° region would reduce the maximum error to ~0.5% or ±2 W m^{-2}.

An analysis using similar correlative data showed that the greatest misclassifications occurred for partly and mostly cloudy scenes. Over mid-latitude land, the mean instantaneous daytime value of F_{clr} may be overestimated by 6 W m^{-2} due to interpretation of clear, cold-air outbreaks as partly cloudy situations. A 1 W m^{-2} underestimate of the clear-sky reflected shortwave flux was also determined for the same areas. The rms errors in the clear-sky longwave and shortwave results appear to be negligible when considered over the entire month. Over tropical and subtropical ocean regions, the clear-sky shortwave flux may be overestimated on average by less than 2 W m^{-2}. A negligible bias error in the daytime, clear-sky longwave flux was found for the same regions. In another study by D. L. Hartmann and D. Doelling (On the net radiative effectiveness of clouds, submitted to *Journal of Geophysical Research*, 1990), evidence suggests that the nighttime, clear-sky longwave flux over the oceans may be overestimated by about 6–7 W m^{-2}, leading to an average overestimate in F_{clr} over the oceans of ~3 W m^{-2} when combining day and night results.

Stuhlmann and Raschke [1987] examined the uncertainties in instantaneous shortwave flux retrievals due to errors in the bidirectional reflectance models for several scene types. They found rms uncertainties of ~42 W m^{-2} for an average ERBE pixel. Averaging over space and time, assuming one fifth of the pixels are independent, gives an rms uncertainty of ~2 W m^{-2} in the monthly mean reflected shortwave flux. The rms uncertainty for the mean longwave flux due to limb-darkening errors is negligible.

Based on a rigorous comparison of April 1985 ERBE results with Geostationary Operational Environmental Sat-

TABLE 3. Effect of Snow on Cloud Forcing

Date	Cloud Forcing Product*	Longwave, W/m^2	Shortwave, W/m^2	Net, W/m^2
April 1985	CF	31.3	−45.1	−13.8
	ΔCF	−1.0	−1.0	−2.0
July 1985	CF	30.1	−46.7	−16.6
	ΔCF	−0.3	0.3	0.0
Oct. 1985	CF	32.2	−50.1	−17.9
	ΔCF	−0.1	−0.7	−0.8
Jan. 1986	CF	30.6	−51.7	−21.1
	ΔCF	−0.6	−0.3	−0.9

*CF is the ERBE cloud forcing parameter; ΔCF is the change in the cloud forcing parameter due to assuming zero cloud forcing over snow.

ellite (GOES) data, an uncertainty of ~1 ± 3 W m^{-2} was estimated in the monthly mean regional, total shortwave flux due to sampling deficiencies. The corresponding errors in total longwave flux were 0 ± 1 W m^{-2}. The errors in net radiation for those results are consistent with preflight assessments of the uncertainties for a two-satellite ERBE [*Brooks and Minnis*, 1984]. *Rieland* [1989], using Meteosat data in a similar study, found rms errors of ~2 W m^{-2} and 5 W m^{-2} in the total longwave and shortwave fluxes, respectively. The corresponding bias errors were less than 1 W m^{-2} for both fluxes. From these two studies the rms errors due to sampling range from 1 to 2 W m^{-2} and 3–5 W m^{-2} for the longwave and shortwave fluxes, respectively.

It is expected that the rms sampling errors for clear-sky shortwave and longwave fluxes are less than the values for total flux, since cloud variability is the main source of error in the total flux. Initial examination of the temporal averaging results for clear-sky albedo indicates that the clear-sky reflected flux is biased by less than 1 W m^{-2}. The potential bias in clear-sky longwave flux over land due to scene misclassification as noted above may be diminished in the temporal averaging due to a change in the averaging procedures. The new process uses some scenes identified as partly cloudy at night in the clear-sky flux averaging. The result of this approach is a significant reduction in the monthly mean clear-sky flux over land and desert areas.

Using the results of these various studies, bias errors for the monthly mean regional total fluxes are less than 1 W m^{-2}. Assuming complete statistical independence of the various error sources, the rms uncertainties in the total longwave and shortwave fluxes are estimated to be 3 W m^{-2} and 5 W m^{-2}, respectively. In terms of shortwave albedo, the error is approximately ±0.014. The rms errors in the clear-sky longwave and shortwave fluxes are estimated to be 2 W m^{-2}. The clear-sky longwave fluxes, however, may be overestimated by ~4 W m^{-2}. The clear-sky reflected flux appears to be overestimated by approximately 1 W m^{-2}. These estimates are based on results which do not adequately cover all conditions. Areas with ice and snow, as well as the western Pacific and Indian Ocean regions, have not been included. Potential errors in the fluxes over snow and ice regions were discussed earlier in this study. More comprehensive ERBE error analyses now in progress will provide more definite values for the ERBE monthly mean products. The errors derived here represent the best estimates to date.

Since net cloud forcing depends on the difference between the absorbed and emitted fluxes, the rms errors in those quantities may either cancel or combine. Thus an additive combination of the regional rms errors would suggest that in the worst case, a given regional value of C is accurate to ± 12 W m^{-2}. More typically, the regional value of C is accurate to ± 7 W m^{-2}, if statistical independence is assumed for each variable. On a global basis, these regional rms errors should be eliminated by averaging. If the preliminary evidence that F_{clr} is overestimated by 4 W m^{-2} and that the clear-sky reflected flux is overestimated by 1 W m^{-2} is confirmed, then both the regional and global results may be biased by 5 W m^{-2}, since there is no compensation apparent in currently available analyses. An overestimate of F_{clr} and α_{clr} causes an equal overestimate in C_{LW} and C_{SW} if all other parameter values are fixed. Net cloud forcing is also increased by an amount equal to the combined overestimate in the two clear-sky quantities. Thus the regional and global values of C reported here may be 5 W m^{-2} too high.

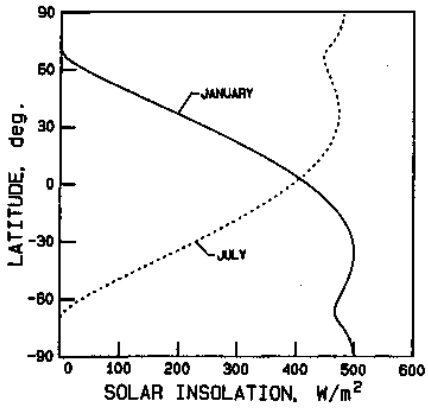

Fig. 2. Latitudinal variation of solar insolation for July and January.

Discussion

Insolation Dependency

Seasonal variations in SW cloud forcing are greatest over oceans in the middle and high latitudes, although marine cloudiness changes only slightly with season between 40° and 70° latitudes in both hemispheres [*Hahn et al.*, 1982]. The seasonal fluctuations in C_{SW} therefore are strongly affected by the annual cycle of solar insolation at the top of the atmosphere for a given latitude (Figure 2). The maximum values of solar insolation occur between 30° and 90° latitude in the summer hemisphere. Figure 3 illustrates the impact of seasonal differences in solar insolation on SW flux for both clear sky and total scene using ERBE results for ocean regions at 60°N and 60°S latitude during January 1986. The difference between the clear-sky and total SW monthly mean fluxes is only −12 W m^{-2} at 60°N latitude (Figure 3*a*). Solar irradiance is very small at this latitude during January. However, at 60°S (Figure 3*b*), the difference is about −140 W m^{-2}. At this latitude, the average irradiance for January is 10 times larger than for 60°N. Total scene albedos (Plate 1*d*) and cloudiness (as derived from the method of *Wielicki and Green* [1989]) are approximately the same over both regions. Daily solar illumination at 60°S lasts for nearly 18 hours in January compared to about 6 hours at 60°N. Although cloud characteristics may also play a role, these large discrepancies in C_{SW} are primarily due to the differences in solar insolation.

Since the LW cloud forcing is ~30 W m^{-2} for both regions,the differences in the net cloud forcing are equal to the difference in C_{SW}, −128 W m^{-2}. From these examples, it is evident that, for a given situation, there may be cooling or warming by clouds, depending on the insolation. This effect plus the predominance of dark ocean surfaces in the southern hemisphere is most likely responsible for the maximum cloud cooling occurring in the southern hemisphere in January as suggested by *Cess and Potter* [1987].

Cloud Types

The clouds responsible for the large values of negative net cloud forcing in the mid-latitudes are probably a mixture of

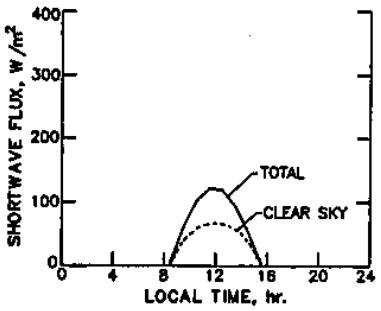

Fig. 3a

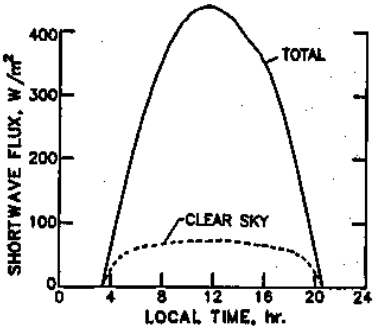

Fig. 3b

Fig. 3. Monthly mean hourly total and clear-sky SW flux for January 1986 from ERBE for ocean regions at (*a*) 60°N and (*b*) 60°S latitude.

low, middle, and high decks near the coasts which are associated with cyclonic activity. Extensive fields of low stratus and stratocumulus clouds are commonly seen in satellite photographs over these areas after the passage of a cyclone. The frequency of occurrence of low, stratiform cloud cover reaches a maximum over these areas [*Hahn et al.*, 1982].

In the tropics the seasonal variations in insolation have much less effect than in the mid-latitudes. Tropical convection centers and the subtropical highs between them govern the seasonal variations of cloud forcing. For example, during July, $C < 0$ over the centers of the regions in central America, southeastern Asia, sub-Sahelian Africa, and Indonesia with the strongest convective activity. Optically thick, dense cloud cover in these areas would lead to the very high albedos shown in Plate 1*b*. On the perimeters of these areas, C becomes quite small and even significantly positive. Optically thin cirrus and midlevel cloud outflows probably cause the positive cloud forcing along these convective fringes. This cirrus effect is especially prominent in the western Pacific during both months. The areas of positive cloud forcing west of north Africa and Mexico during January coincide with maxima in the frequency of occurrence of cirrus and midlevel clouds without any other clouds present [*Hahn et al.*, 1982]. Without optically thick low clouds beneath cirrus, there is insufficient reflection to compensate for the cirrus greenhouse effect.

The widespread marine stratocumulus clouds associated with the eastern halves of the subtropical highs are responsible for the largest negative values of net cloud forcing in the tropics. While these features nearly disappear from the northern hemisphere during winter, they are easily observed west of South America, Africa, and Australia during both months. The high frequency of coincident cumulus and cirrus on the western sides of the subtropical highs [*Hahn et al.*, 1982] and the lack of extensive cloud cover apparently produce negligible cloud forcing over those areas (Plates 5*a* and 5*b*).

Over land, the impact of clouds on the net radiation budget is usually less than the adjacent ocean regions. This difference may be due to several effects. On average, there appears to be less cloudiness over land; hence there is less cloud forcing. The SW contrast between the clouds and the surface is also lower over the higher albedo surfaces. Thus C_{SW} would be lower over bright land areas than over water for the same cloud cover. A greater incidence of cirrus and fewer occurrences of low clouds over land relative to the oceans in the mid-latitudes [see *Hahn et al.*, 1982, 1984] would also lead to cancellation of C_{SW} by C_{LW}. Over regions such as the North American Great Plains, the Tibetan Plateau, central Australia, Mongolia, and the western Sahara Desert, the observed positive net cloud forcing in January (Plate 5*b*) is collocated with maxima in the climatological occurrence of cirrus by itself [*Hahn et al.*, 1984]. The areas of negative net forcing over the northern hemisphere during January (e.g., China, Great Lakes) are coincident with relative maxima in the occurrence of low-level stratiform clouds and minima in cirrus by itself. Convective centers over South America and South Africa produce abundant cloudiness with high albedos (cloud fraction >0.8, $\alpha > 30\%$), yielding large values of C_{SW}. Thus the net cloud forcing is generally negative in January over those areas. During July, the presence of vegetated land at high northern latitudes and the insolation effect result in extensive areas of negative cloud forcing. The general lack of cloudiness over the major deserts and the Brazilian savannahs during July leads to negligible cloud forcing.

Comparisons With GCMs

Zonal means of C_{LW}, C_{SW}, and C from ERBE are shown with those computed with two GCMs for January in Figures 4*a*, 4*b*, and 4*c*, respectively. The model results are from the modified National Center for Atmospheric Research Community Climate Model (modified NCAR CCM) [see *Charlock and Ramanathan*, 1985] and the Oregon State University/Lawrence Livermore National Laboratory (OSU/LLNL) GCM [see *Cess and Potter*, 1987]. In general, the ERBE values of LW cloud forcing lie between the results from the two models (see Figure 4*a*). The latitudinal variations of C_{LW} from the OSU/LLNL GCM are more extreme than the observations, while the modified NCAR CCM results are relatively insensitive to latitude. The greatest differences in C_{LW} are found over Antarctica, where the ERBE data indicate little or no cloud effect. As noted earlier, the observed cloud effects over snow are subject to greater uncertainty than elsewhere, so little importance should be given to the comparisons over Antarctica. The substantial discrepancies over the deep convective centers at about 10°S, however, suggest the need for improvements in the characterization of tropical cloudiness in the models. Similar differences are found in the comparisons of C_{SW} in Figure 4*b*

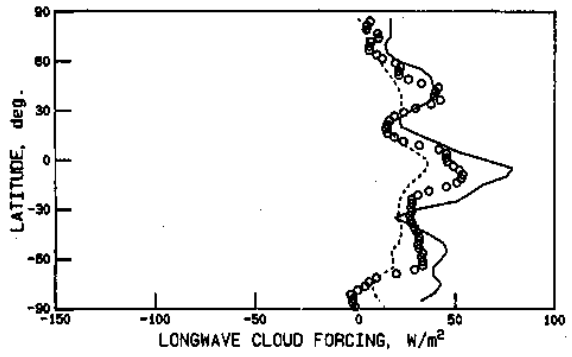

Fig. 4a

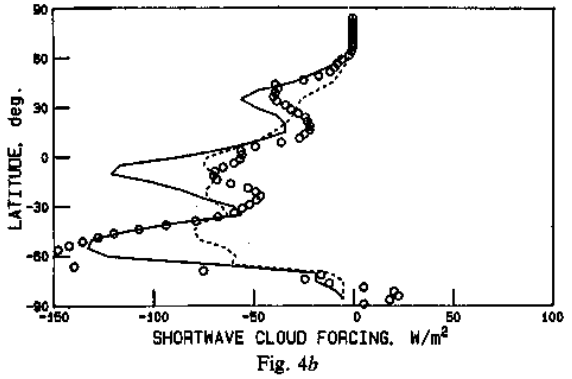

Fig. 4b

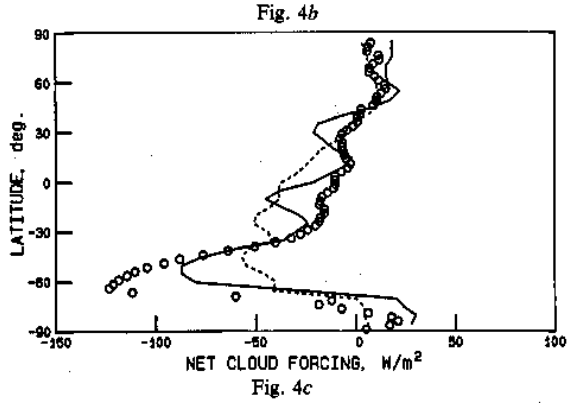

Fig. 4c

Fig. 4. Comparison of (*a*) LW, (*b*) SW, and (*c*) net cloud forcing from ERBE (circles) with calculations from two GCMs (solid line is from *Cess and Potter* [1987]; dashed line is from *Charlock and Ramanathan* [1985]) for January.

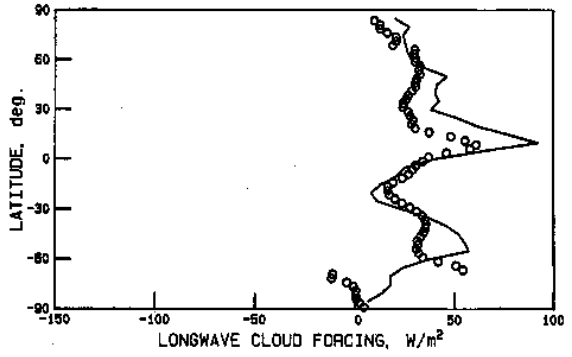

Fig. 5a

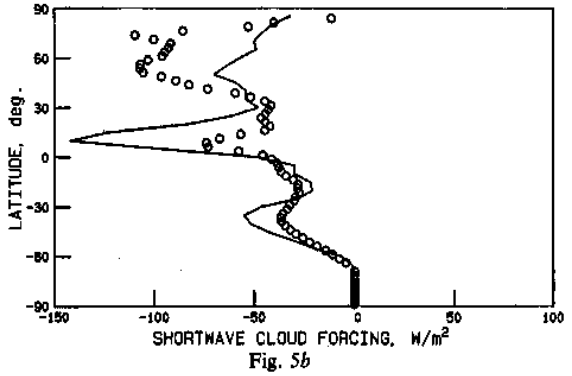

Fig. 5b

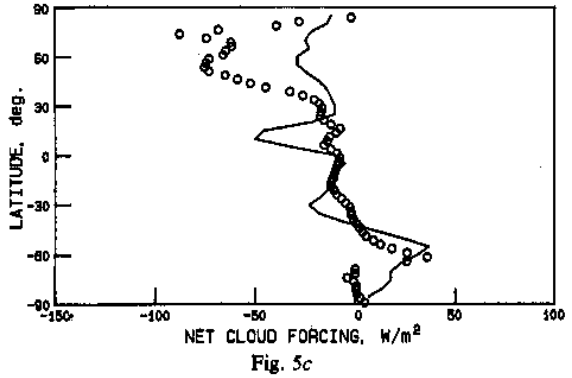

Fig. 5c

Fig. 5. Comparison of (*a*) LW, (*b*) SW, and (*c*) net cloud forcing from ERBE (circles) with GCM calculations (solid line) from *Cess and Potter* [1987] for July.

except that both models tend to overestimate the magnitude of the negative SW cloud forcing in the tropics. Comparison of net cloud forcing between ERBE data and the two models (Figure 4c) shows good agreement in C north of 40°N, overestimation of the cooling by the models in the tropics, and underestimation of net cooling in the southern mid-latitudes. The global mean net forcing agrees to within 2 W m^{-2} for the three data sets. This result is like that found by *Cess and Potter* [1987] in that, overall, the models and observations agree, but for the wrong reasons.

A similar comparison is shown in Figure 5 for July 1985, using ERBE and the results from *Cess and Potter* [1987]. Again, the largest differences in both C_{LW} and C_{SW} are over the convective centers at about 10°N. The negative SW cloud forcing over the northern mid-latitudes is underestimated by ~50 W m^{-2}. The net result (Figure 5c) is an underestimation of the magnitude of net cloud forcing north of 30°N in the model. This underestimation by the model translates to a difference of 5 W m^{-2} in the global mean net cloud forcing.

The regional observations shown in Plates 1 and 2 for January 1986 may be compared qualitatively to the NCAR Community Climate Model (CCM1) results for January given in Figures 1 and 2 of *Slingo and Slingo* [1988]. The CCM1 clear-sky albedos and LW fluxes agree well with the ERBE results presented here. Total albedos and LW fluxes north of 30°N are also very similar to the ERBE results both in magnitude and location. In the southern hemisphere, however, the model extrema differ considerably from the observations in both size and position. For example, the minima in α are found over the marine stratus areas in the model results. The ERBE data have relative maxima in those regions. Conversely, the areas of sparse cloud cover in the Pacific with $\alpha < 20\%$ in the observations have values of $\alpha >$

TABLE 4. Comparison of ERBE Cloud Radiative Forcing and GCM Predictions

Reference	Model	Cloud Radiative Forcing, W/m^2		
		Longwave	Shortwave	Net
Herman et al. [1980]	GLAS GCM, Jan.	40	−54	−14
Charlock and Ramanathan [1985]	Modified NCAR CCM, Jan.	23	−45	−22
Ramanathan [1987]	NCAR CCM, Jan.	35	−57	−22
Randall and Harshvardhan [1986]	UCLA/Goddard GCM, Jan.	55	−57	−2
	UCLA/Goddard GCM, July	53	−52	+1
J.F.B. Mitchell [in *Cess and Potter*, 1987]	UKMO GCM, Jan.	40	−74	−34
	UKMO GCM, July	42	−69	−27
Cess and Potter [1987]	OSU/LLNL GCM, Jan.	42	−62	−20
	OSU/LLNL GCM, July	39	−52	−13
Slingo and Slingo [1988]	NCAR CCM1, Jan.	30	−51	−21
This work	ERBE, Jan.	31	−52	−21
	ERBE, July	30	−47	−17

20% in the CCM1 results. These overestimates of albedo in the tropics are balanced by underestimates of albedo over many parts of the ITCZ and the mid-latitude storm tracks. Overall, however, $C_{SW} = -51$ W m^{-2} for the CCM1 results averaged over the globe. Similar, though less obvious, differences are evident in a comparison of the ERBE and CCM1 regional values of C_{LW}. The regional differences balance out, so that $C_{LW} = 30$ W m^{-2}. Thus the global SW, LW, and net values of cloud forcing from the CCM1 are in quite good agreement with the ERBE results for January. Here again, the model and measured data agree due to cancellation of disagreements.

A summary comparison of the global cloud forcing parameters derived from the ERBE data and from several GCM calculations [*Cess and Potter*, 1987] is presented in Table 4. This comparison includes model results from *Herman et al.* [1980], *Charlock and Ramanathan* [1985], *Ramanathan* [1987], *Randall and Harshvardhan* [1986], *Slingo and Slingo* [1988], and J. F. B. Mitchell (unpublished data, but included in *Cess and Potter* [1987]). The ranges of fluctuation in values for C_{LW}, C_{SW}, and C are 32, 29, and 35 W m^{-2}, respectively. The ERBE data fall in the middle of the model results. Since *Cess and Potter* [1987] explained the numerous differences in these model results, they will not be repeated here.

Summary and Conclusions

The ERBE data represent the most complete and accurate depiction of the Earth's total and clear-sky radiation budget at the top of the atmosphere. Monthly averaged clear-sky and total flux data from the ERBE were used to assess the impact of clouds on the Earth's radiation budget. This impact was examined in terms of three quantities: LW, SW, and net cloud forcing. Overall, clouds cool the Earth-atmosphere system by 17 W m^{-2}. The global mean cooling varied from 14 to 21 W m^{-2} between April 1985 and January 1986. Seasonal variations in LW cloud forcing are relatively small, the maximum range corresponding to the annual migration of the ITCZ. Maximum seasonal variations of SW and net cloud forcing occur in the mid-latitudes driven by the annual insolation cycle.

The main factors determining whether clouds cause a radiative excess or deficit in a given region are insolation, cloud amount, cloud type (height and phase), and surface properties. Numerous theoretical studies have shown that any changes in one or more of these variables will produce a change in cloud forcing. By far, the strongest effects of clouds are found in the mid-latitude storm tracks over the oceans. A shift in the position and/or intensity of the mid-latitude cyclones by some other climate forcing variable (e.g., CO_2) could have a significant effect on the cloud forcing of the system. Outside the storm tracks, there are significant areas where LW warming is balanced by SW cooling. Cirrus and marine stratocumulus clouds appear to have the most impact on the radiation balance. Areas dominated by one cloud type or the other are highlighted in the tropics by relative minima and maxima in net cloud forcing. Any change in climate which affects the relative distributions of these cloud types will change the cloud forcing, especially in the tropics.

Estimation of changes in climate due to one variable or another requires the use of model calculations. Modeled regional and zonal values of net cloud forcing show a need for considerable improvement. Since there appears to be good agreement between modeled and observed clear-sky fluxes, it is evident that the parameterizations of cloud amount, type, and optical properties used in the various GCMs are inadequate at this point. Improvements in our basic understanding of cloud processes is imperative to supplement the model cloud schemes. Programs such as the International Satellite Cloud Climatology Project (ISCCP [see *Schiffer and Rossow*, 1983]) and the first ISCCP Regional Experiment (FIRE) [*Starr*, 1987], have been implemented to enhance our knowledge of cloud systems, especially cirrus and marine stratocumulus. With the FIRE and other research results, it should be possible in the near future to realize higher accuracies in model-predicted climate changes.

Acknowledgments. The contributions of F. M. Denn and D. F. Young of Lockheed Engineering and Sciences Company to the analysis and graphical presentation of the data are gratefully acknowledged. We would like to thank J. F. Kibler of NASA Langley and the ERBE Data Management Team for their efforts in processing the ERBE data and making the appropriate data products available for scientific use. We would also like to express our appreciation to O. C. Smith of ST Systems Corporation for computer programing and analysis support in the production of the ERBE output products and in validation of the ERBE data. Finally, we would like to extend our sincere thanks to the anonymous reviewers for their valuable suggestions.

REFERENCES

Barkstrom, B. R., The Earth Radiation Budget Experiment (ERBE), *Bull. Am. Meteorol. Soc.*, *65*, 1170–1185, 1984.

Barkstrom, B. R., and G. L. Smith, The Earth Radiation Budget Experiment: Science and implementation, *Rev. Geophys.*, *24*, 379–390, 1986.

Barkstrom, B. R., E. Harrison, G. Smith, R. Green, J. Kibler, R. Cess, and the ERBE Science Team, Earth Radiation Budget Experiment (ERBE) archival and April 1985 results, *Bull. Am. Meteorol. Soc.*, *70*, 1254–1262, 1989.

Briegleb, B. P., P. Minnis, V. Ramanathan, and E. F. Harrison, Comparison of clear-sky albedos inferred from satellite observations and model computations, *J. Clim. Appl. Meteorol.*, *25*, 214–226, 1986.

Brooks, D. R., and P. Minnis, Simulation of the Earth's monthly average regional radiation budget derived from satellite measurements. *J. Clim. Appl. Meteorol.*, *23*, 392–403, 1984.

Brooks, D. R., E. F. Harrison, P. Minnis, J. T. Suttles, and R. S. Kandel, Development of algorithms for understanding the temporal and spatial variability of the earth's radiation balance, *Rev. Geophys.*, *24*, 422–438, 1986.

Cess, R. D., Climate change: An appraisal of atmospheric feedback mechanisms employing zonal climatology, *J. Atmos. Sci.*, *33*, 1831–1843, 1976.

Cess, R. D., and G. L. Potter, Exploratory studies of cloud radiative forcing with a general circulation model, *Tellus*, *39A*, 460–473, 1987.

Charlock, T. P., and V. Ramanathan, The albedo field and cloud radiative forcing produced by a general circulation model with internally generated cloud optics, *J. Atmos. Sci.*, *42*, 1408–1429, 1985.

Dewey, K. F., Satellite-derived maps of snow cover frequency for the northern hemisphere, *J. Clim. Appl. Meteorol.*, *26*, 1210–1229, 1987.

Diekmann, F. J., and G. L. Smith, Investigation of scene identification algorithms for radiation budget measurements, *J. Geophys. Res.*, *94*, 3395–3412, 1989.

Hahn, C. J., S. G. Warren, J. London, R. M. Chervin, and R. Jenne, Atlas of simultaneous occurrence of different cloud types over the ocean, Natl. Cent. for Atmos. Res., Boulder, Colo., *Tech. Note NCAR/TN-201+STR*, 212 pp., Nov. 1982.

Hahn, C. J., S. G. Warren, J. London, R. M. Chervin, and R. Jenne, Atlas of simultaneous occurrence of different cloud types over land, Natl. Cent. for Atmos. Res., Boulder, Colo., *Tech. Note NCAR/TN-241+STR*, Aug. 1984.

Harrison, E. F., D. R. Brooks, P. Minnis, B. A. Wielicki, W. F. Staylor, G. G. Gibson, D. F. Young, F. M. Denn, and the ERBE Science Team, First estimates of the diurnal variation of longwave radiation from the multiple-satellite Earth Radiation Budget Experiment (ERBE), *Bull. Am. Meteorol. Soc.*, *69*, 1144–1151, 1988.

Hartmann, D. L., V. Ramanathan, A. Berroir, and G. E. Hunt, Earth radiation budget data and climate research, *Rev. Geophys.*, *24*, 439–468, 1986.

Herman, G., M.-L. Wu, and W. Johnson, The effects of clouds on the earth's solar and infrared radiation budgets, *J. Atmos. Sci.*, *37*, 1251–1261, 1980.

Hwang, P. H., L. L. Stowe, H. Y. M. Yeh, H. L. Kyle, and Nimbus-7 Cloud Data Processing Team, The Nimbus-7 global cloud climatology, *Bull. Am. Meteorol. Soc.*, *69*, 743–752, 1988.

Kopia, L. P., Earth Radiation Budget Experiment scanner instrument, *Rev. Geophys.*, *24*, 400–406, 1986.

Minnis, P., and E. F. Harrison, Diurnal variability of regional cloud and clear-sky radiative parameters derived from GOES data, III, November 1978 radiative parameters, *J. Clim. Appl. Meteorol.*, *23*, 1032–1051, 1984.

Ohring, G., and P. Clapp, The effect of change in cloud amount on the net radiation at the top of the atmosphere, *J. Atmos. Sci.*, *37*, 447–454, 1980.

Ramanathan, V., The role of Earth radiation budget studies in climate and general circulation research, *J. Geophys. Res.*, *92*, 4075–4095, 1987.

Ramanathan, V., R. D. Cess, E. F. Harrison, P. Minnis, B. R. Barkstrom, E. Ahmad, and D. Hartmann, Cloud-radiative forcing and climate: Results from the Earth Radiation Budget Experiment, *Science*, *243*, 57–63, 1989.

Randall, D. A., and Harshvardhan, Cloud radiative forcing in a general circulation, paper presented at the Sixth Conference on Atmospheric Radiation, Am. Meteorol. Soc., Williamsburg, Va., 1986.

Rieland, M., Stichprobenanalysen des Tagesganges der planetaren Strahlungsbilanz, Ph.D. dissertation, 117 pp., Univ. Köln, Dep. of Math. Nat. Sci., Federal Republic of Germany, 1989.

Schiffer, R. A., and W. B. Rossow, The International Satellite Cloud Climatology Project (ISCCP): The first project of the World Climate Research Program, *Bull. Am. Meteorol. Soc.*, *64*, 779–784, 1983.

Slingo, A., and J. M. Slingo, The response of a general circulation model to cloud longwave radiative forcing, I, Introduction and initial experiments, *Q. J. R. Meteorol. Soc.*, *114*, 1027–1062, 1988.

Smith, G. L., R. N. Green, E. Raschke, L. M. Avis, B. A. Wielicki, and R. Davies, Inversion methods for satellite studies of the earth's radiation budget, *Rev. Geophys.*, *24*, 407–421, 1986.

Somerville, R. C. J., and L. A. Remer, Cloud optical thickness feedbacks in the CO_2 climate problems, *J. Geophys. Res.*, *89*, 9668–9672, 1984.

Starr, D. O'C., A cirrus-cloud experiment: Intensive field observations planned for FIRE, *Bull. Am. Meteorol. Soc.*, *68*, 119–124, 1987.

Stuhlmann, R., and E. Raschke, Satellite measurements of the earth radiation budget: Sampling and retrieval of shortwave exitances—A sampling study, *Contrib. Phys. Atmos.*, *60*, 393–410, 1987.

Suttles, J. T., R. N. Green, P. Minnis, G. L. Smith, W. F. Staylor, B. A. Wielicki, I. J. Walker, D. F. Young, V. R. Taylor, and L. L. Stowe, Angular radiation models for earth-atmosphere system, vol. 1, Shortwave radiation, *NASA RP-1184*, 1988.

Suttles, J. T., R. N. Green, G. L. Smith, B. A. Wielicki, I. J. Walker, V. R. Taylor, and L. L. Stowe, Angular radiation models for earth-atmosphere system, vol. 2, Longwave radiation, *NASA RP-1184*, 1989.

Wielicki, B. A., and R. N. Green, Cloud identification for ERBE radiative flux retrieval, *J. Appl. Meteorol.*, *28*, 1133–1146, 1989.

B. R. Barkstrom, E. F. Harrison, and P. Minnis, Atmospheric Sciences Division, NASA Langley Research Center, Hampton, VA 23665.

R. D. Cess, Laboratory for Planetary and Atmospheric Research, State University of New York at Stony Brook, Stony Brook, NY 11794.

G. G. Gibson, Lockheed Engineering and Sciences Company, Hampton, VA 23666.

V. Ramanathan, Department of Geophysical Sciences, University of Chicago, Chicago, IL 60637.

(Received June 29, 1989;
revised March 23, 1990;
accepted May 9, 1990.)